The GALILEO γ-ray array at the Legnaro National Laboratories

A. Goasduff[a,b,c], D. Mengoni[b,c], F. Recchia[b,c], J. J. Valiente-Dobón[a], R. Menegazzo[c], G. Benzoni[d], D. Barrientos[a], M. Bellato[c], N. Bez[c], M. Biasotto[a], N. Blasi[d], C. Boiano[d], A. Boso[b,c], S. Bottoni[d,e], A. Bracco[d,e], S. Brambilla[d], D. Brugnara[b,a], F. Camera[d,e], S. Capra[d,e], A. Capsoni[d], P. Cocconi[a], S. Coelli[d], M. L. Cortés[a,f], F.C.L. Crespi[d,e], G. de Angelis[a], F. J. Egea[a,b,c], C. Fanin[c], S. Fantinel[a], A. Gadea[g], E. R. Gamba[d,e], A. Gambalonga[a], C. Gesmundo[d], G. Gosta[d,e], A. Gottardo[a], A. Gozzelino[a], E. T. Gregor[a], M. Gulmini[a], J. Ha[b,c], K. Hadyńska-Klęk[a,h], A. Illana[a,i], R. Isocrate[c], G. Jaworski[a,h], P. R. John[b,c,f], S. M. Lenzi[b,c], S. Leoni[d,e], S. Lunardi[b], M. Magalini[b], N. Marchini[j,l], B. Million[d], V. Modamio[k], A. Nannini[l], D. R. Napoli[a], G. Pasqualato[b,c], J. Pellumaj[a,m], R. M. Pérez-Vidal[a], S. Pigliapoco[b,c], M. Polettini[d,e], C. Porzio[d,e], A. Pullia[d,e], L. Ramina[c], G. Rampazzo[c], M. Rampazzo[c], M. Rebeschini[c], K. Rezynkina[c], M. Rocchini[l,o], M. Romanato[c], D. Rosso[a], A. Saltarelli[j,1], M. Scarcioffolo[b,c], M. Siciliano[a,p], D. A. Testov[b,c,q,r], D. Tomasella[b], F. Tomasi[d], N. Toniolo[a], C. A. Ur[c,r], S. Ventura[c], F. Veronese[c], E. Viscione[d], V. Volpe[a], O. Wieland[d], I. Zanon[a,m], S. Ziliani[d,e], G. Zhang[b,c], and D. Bazzacco[c]

[a] *INFN Laboratori Nazionali di Legnaro, Legnaro, Italy*
[b] *Dipartimento di Fisica e Astronomia, Università di Padova, Padova, Italy*
[c] *INFN Sezione di Padova, Padova, Italy*
[d] *INFN Sezione di Milano, Milano, Italy*
[e] *Dipartimento di Fisica, Università degli Studi di Milano, Milano, Italy*
[f] *Institut für Kernphysik, Technische Universität Darmstadt, Darmstadt, Germany*
[g] *IFIC, CSIC-Universitat Valencia, Valencia, Spain*
[h] *Heavy Ion Laboratory, University of Warsaw, Warsaw, Poland*
[i] *University of Jyvaskyla, Department of Physics, P.O. Box 35, FI-40014 University of Jyvaskyla, Finland.*
[j] *Physics Division, Università degli Studi di Camerino, Camerino, Italy.*
[k] *Department of Physics, University of Oslo, N-0316 Oslo, Norway*
[l] *INFN Sezione di Firenze, Firenze, Italy*
[m] *Dipartimento di Fisica e Scienze della Terra, Università di Ferrara, Ferrara, Italy.*
[n] *INFN Sezione di Perugia, Camerino, Italy.*
[o] *Department of Physics, University of Guelph, Guelph, Canada.*
[p] *Physics Division, Argonne National Laboratory, Argonne, USA*
[q] *Joint Institute for Nuclear Research, Dubna, Russia*
[r] *Extreme Light Infrastructure - Nuclear Physics, IFIN-HH, Bucharest-Magurele, Romania*

Abstract

GALILEO, a new 4π high-resolution γ-detection array, based on HPGe detectors, has been developed and installed at the Legnaro National Laboratories. The GALILEO array greatly benefits from a fully-digital read-out chain, customized DAQ, and a variety of complementary detectors to improve the resolving power by the detection of particles, ions or high-energy γ-ray transitions. In this work, a full description of the array, including electronics and DAQ, is presented together with its complementary instrumentation.

Keywords: high-resolution γ-ray spectroscopy, HPGe, silicon, neutron, electronics, DAQ

1. Introduction

GALILEO is the resident array for advanced in-beam γ-ray spectroscopy studies constructed and installed at the Legnaro National Laboratories (LNL), INFN, Italy. Gamma-ray spectroscopy realised with GALILEO takes advantage of reactions induced by the stable beams delivered by the Tandem-ALPI-PIAVE accelerator complex [1] and by radioactive beams that will be provided by the SPES facility [2] in the near future. GALILEO is a 4π high-resolution array which combines the GASP [3] High-Purity Germanium (HPGe) tapered detectors and HPGe capsules of the EUROBALL [4] Cluster detectors mounted in a common cryostat accommodating three encapsulated HPGe crystals, the so-called GALILEO triple-cluster (GTC) detectors.

The geometry of the array is designed to maximize the photo-peak efficiency under typical in-beam medium-high γ-ray multiplicity conditions, achieving a value of 4.5% at 1332 keV. The HPGe detectors are surrounded by anti-Compton shields to reach a peak-to-total ratio (P/T) of about 50% for the whole array using a ^{60}Co source. A thick Pb shield improves Compton rejection, avoiding direct γ-ray interactions in the BGO shields.

A large selection of ancillary detectors has been developed to be coupled to GALILEO in order to improve its sensitivity. This allows the investigation of a wide variety of physical phenomena, including shell evolution, shape coexistence and deformation in neutron-rich and neutron-deficient nuclei, isospin symmetry breaking at zero and non-zero temperatures, alpha clustering and near threshold states, or properties of the nuclei of interest for the astrophysical slow and rapid neutron-capture processes (s- and r-process).

In this article, we present the GALILEO array, its ancillary instrumentation and performances. The article is organised as follows: Section 2 describes the GALILEO infrastructure, in Section 3 the custom electronics developed for the HPGe read-out is detailed, while the data acquisition environment is outlined in Section 4. Performances and simulations of the array are given in Section 5, while the ancillary detectors that can be coupled to GALILEO are presented in Section 6.

2. GALILEO Infrastructure

The GALILEO project has been divided in two phases: *GALILEO Phase I*, consisting of up to 25 single GASP HPGe tapered detectors, equipped with anti-Compton shields, and *GALILEO Phase II*, where 10 triple cluster detectors were added to the *Phase I*, reaching the project nominal efficiency and solid angle coverage.

2.1. GALILEO Phase I

The GALILEO γ-ray spectrometer, in its Phase I realization, was composed of 25 Compton-suppressed HPGe tapered detectors placed at 235 mm from the interaction point, as shown in the top panel of Fig. 1. The total measured photo-peak efficiency was ~2.1% at 1332 keV and the P/T ~55%. The energy resolution was 0.17% at 1332-keV transition of ^{60}Co calibration source (FWHM = 2.3 keV).

The HPGe detectors and their anti-Compton shields were the same of the γ-ray array GASP [3, 5]. They are composed of a coaxial hyperpure crystal with ~82 mm length and ~ 72 mm diameter. The crystals are tapered in the front ~30 mm of their length, with a cone of 10°. The average relative efficiency, defined for the 1332 keV radiation with respect to a 3×3 inch NaI(Tl) scintillator at 250 mm from the source, is 82%.

Table 1: Position and efficiency of the HPGe detectors in the two GALILEO configurations: second column shows the number of detectors at each azimuthal angle (third columns), while the fourth column shows the efficiency for each group of detectors.

Configuration	Number of det.	Theta [deg.]	Efficiency [%]
Phase I	5	152°	0.42
	5	129°	0.42
	5	119°	0.42
	10	90°	0.84
Phase II	5	149°	1.17
	5	118.5°	1.17
	10	90°	0.84
	5	61°	0.42
	5	51°	0.42
	5	28°	0.42

The anti-Compton shield of each GASP detector is composed of eight optically isolated BGO crystals, 195 mm long, coupled to eight photomultipliers tubes. BGO crystals have an average energy resolution of 18% at 661.6 keV, with a noise level lower than 15 keV.

In the Phase I configuration, the 25 tapered detectors were positioned in rings at 152°(5 detectors), 129°(5 detectors), 119°(5 detectors) and at 90°(10 detectors) with respect to the beam axis, as listed in Tab. 1. Each ring was supported by a movable portal that entail an opening of the array along the beam axis. The 3D CAD rendering of the full configuration is shown in the top panel of Fig. 1, where, aided by the exploded representation, the single portals hosting the HPGe detectors are clearly distinguishable. The beam enters from the left side of the figure. The two forward portals were removed for the Phase I to accommodate large-size complementary detectors to provide the necessary selectivity for studying, for example, neutron-deficient nuclei populated in fusion-evaporation reactions where γ rays are typically measured in coincidence with light-charged particles and neutrons.

Ancillary detectors coupled to GALILEO Phase I were EUCLIDES [6] for the detection of light-charged particles emitted in fusion-evaporation reactions, GALTRACE [7] for light particles emitted in direct reactions, SPIDER [8] for ion detection, Neutron Wall [9] for neutrons, the Cologne-LNL plunger [10, 11], and $LaBr_3$:Ce [12] detectors (see Sec. 6). The GALILEO phase I has been running from 2015 to 2020 with more than 30 experiments performed [13, 14, 15, 16, 17, 18, 19, 20, 21, 22, 23, 24, 25].

2.2. GALILEO Phase II

The phase II of the GALILEO expands the project with the addition of ten triple cluster detectors (GTC) and their associated anti-Compton shield (GTC-AC), using existing HPGe and BGO crystals from the EUROBALL array [4, 5] (see Fig. 1, bottom).

The placement of the ten GTC in the array has been chosen to increase the efficiency at angles other than 90°. This implies that Phase II geometry is greatly advantageous for lifetime measurements using techniques based on Doppler shift.

Each crystal of the GTC detectors has a relative efficiency of 60% and is individually encapsulated. The encapsulation is realised by an aluminum case of 0.7 mm thickness which provides a separation between the capsule and cryostat vacuum, and a safe handling of the detector. Each

capsule is 78 mm long with a diameter of 70 mm, and is tapered in its frontal face. For the realisation of the GALILEO triple detectors, three individual capsules are accommodated into a common cryostat, and surrounded by a custom-designed anti-Compton shield using BGO crystals of the 7-fold Cluster detectors of the EUROBALL array. Each anti-Compton shield consists of 9 crystals coupled to twelve photomultipliers.

At variance from the 90-degree ring and forward hemisphere, the lead shield is not used for the GTC detectors, while Hevimet collimators are mounted on the front face of the BGO detectors in order to avoid direct interactions in the crystals and enhance the P/T ratio.

The 3D rendering of the GTC detectors is shown in Fig. 2, together with a detailed view of the geometry of the GTC-AC shields. A gap of 20 mm is present between the front face of the HPGe detectors and the BGO shielding.

The final GALILEO Phase II configuration is composed of: 5 GTC detectors placed at 149° and 5 GTC at 118.5°, in addition to 10 GASP tapered detectors at 90°, 5 GASP at 61°, 5 GASP at 51° and, finally, 5 GASP at 28°. GTC are placed at 245 mm from the target. Polar angles and efficiency for each ring are listed in Tab. 1.

The overall gain in efficiency for GALILEO Phase II is more than a factor of two with respect to the Phase I, increasing from 2.1% to 4.5%.

2.3. GALILEO mechanics

The two phases of the GALILEO project share the same mechanical infrastructure, that is distributed in separate and independent parts: two shells, upstream and downstream, and a ring between them, whose geometrical centre represents the centre of the array. The upstream shell is a solid hemisphere accommodating up to 15 single crystal detectors in the Phase I, and 10 GTC detectors in the Phase II, while the downstream shell is divided in two sub-units, allocating 10 and 5 tapered detectors respectively.

The central portal hosts the Pb collimating shield for the detectors located at 90°and the scattering chamber, which consists of three separate units, resembling the outer structure: two portions of a sphere with a non-uniform radius of ∼12 mm, and a central ring with a radius of 11.6 mm. The scattering chamber is made of thin 2 mm aluminium of series 6000, in order to limit the absorption of low-energy γ rays.

The support of the detectors on the central portal can be adapted to host different kind of detectors, such as 3×3 inch $LaBr_3$:Ce detectors for the measurement of high-energy γ rays.

The beam-dump is placed downstream at ∼3 m from the measuring position, thus reducing the background. Two pumping units are placed upstream and downstream to allow reaching an operational vacuum of 10^{-6} mbar in the scattering chamber.

A specific remote system has been designed to allow the change of the target without opening the scattering chamber. The remote target loading system is based on a moving chariot pulled by a closed-loop stainless-steel wire. The wire is set in motion by two pulleys, one placed at the far end of the beamline (in front of the beamdump) and the free-running one at the entrance of the scattering chamber. The target is placed on an extended stick which is designed to arrive at the centre of the scattering chamber. A stepper motor acts on the far-end pulley to move the chariot from and to the scattering chamber. Proximity sensors provide a feedback signal to the motor. Up to 10 targets/frames can be stored in a dedicated buffer vacuum chamber perpendicular to the beamline, which can be isolated from the main vacuum by a manual all-metal vacuum valve. When a target or frame is to be used, it is moved from the loader to the chariot using a manipulator.

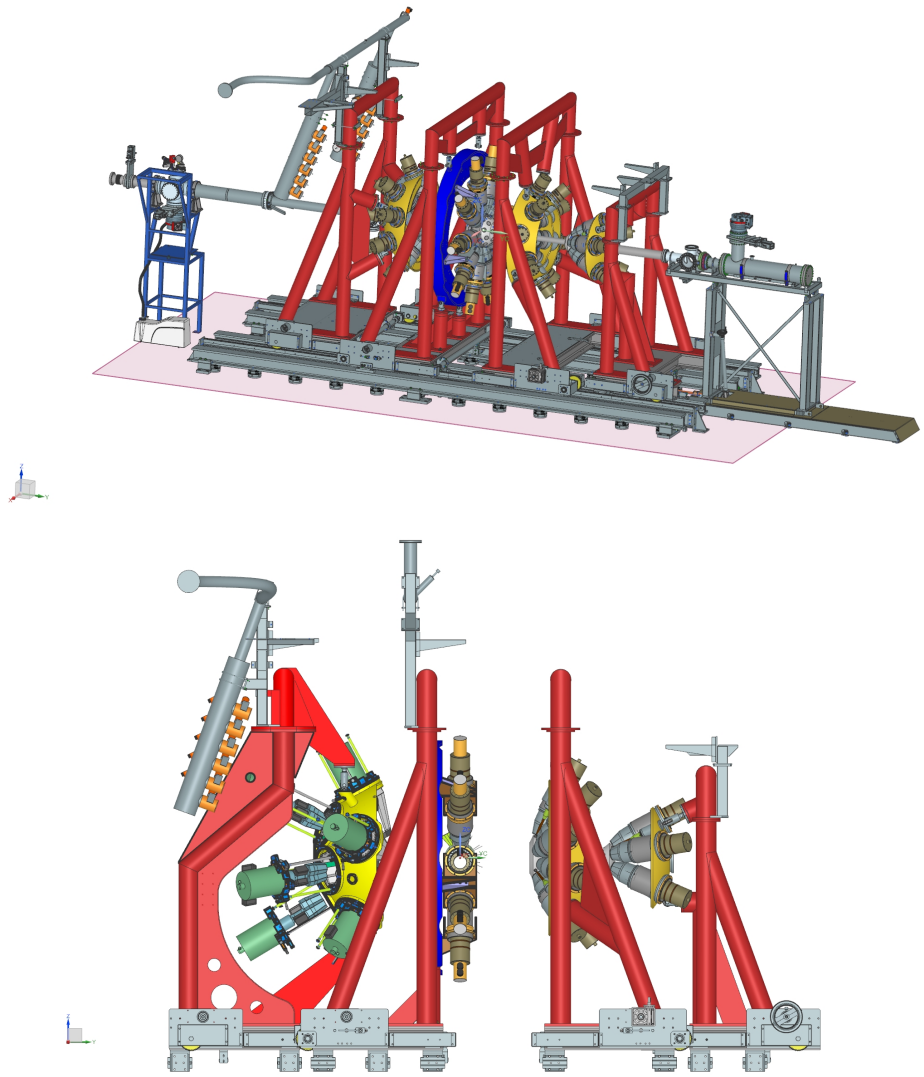

Figure 1: (Color Online) Design drawing of the GALILEO Phase I (top panel) and II (bottom panel) configurations of the GALILEO array. The exploded representation allows to see the portals hosting groups of detectors, and the opening along the beamline. Elements such as manifolds for LN_2 distributions and the downstream beam dump are also clearly visible in the drawings. The beam axis follows from the left to the right in both panels.

3D images of the downstream beamline modified to accommodate the remote handling system are shown in Fig. 3: the top panel shows the layout of the chambers and of the manipulator. The stick holding the target is visible to the far right of the figure, while the bottom panel highlights the buffer vacuum chamber and the support structure within the beamline elements.

The holding structure of devices which needs to be placed inside the scattering chamber (i.e. EUCLIDES, GALTRACE, SPIDER and plunger) is maintained by two short-rail insertions in the central part of the scattering chamber, one at the top and one at the bottom of the central ring. Such insertions are also used to hold a single-stick target holder useful for calibration purposes and in case the remote-target system is not exploited.

3. Electronics

The Front-End Electronics (FEE), developed in collaboration with the Advanced GAmma Tracking Array (AGATA) [26] collaboration, is composed of two main blocks: the analog part with the preamplifiers, and the digital part composed of the digitizers and the preprocessing electronics.

3.1. Preamplifiers

The output of the HPGe detectors is read out by charge-sensitive preamplifiers employing a fast-reset technique for dead time and dynamic range optimization [27, 28]. This technique consists of a fast discharge of the pole-zero capacitance when the preamplifier output signal is larger than a programmable threshold. As the length of the saturated pulse is proportional to the height of the input pulse, the dynamic range of the preamplifiers is thus increased. The differential output of the preamplifiers and the differential signals coming from the BGO scintillators are arranged into 6-way cables connected by MDR connectors at the input of the digitizer modules. The digitizer module has been developed for the upgrade of electronics of the AGATA array [26], and is composed of eight electronic boards: six Digi-Opt12 boards [29] and two Control Cards [30, 31, 32].

3.2. Digitizers and signal processing

The Digi-Opt12 board is a low power 12-channel digitizer board with optical output that performs a digitization of the differential input signals at 100 Msps with a resolution of 14 bits. The digital output is sent to a 12-fiber optical cable by means of high-speed serial links, encoded with the JESD204A protocol [33] and operating at 2 Gbps each.

Each channel has two programmable input ranges, corresponding to energy ranges of 0-7 or 0-20 MeV for γ rays interacting in the HPGe detectors equipped with the GALILEO-type preamplifiers, described in the previous subsection. In addition, the analog offset of each channel is also programmable from the slow control system and a synchronization signal can be injected at the input of the Analog-to-Digital Converters (ADC) to compensate different channel latencies due to unbalanced digital paths. The sampling clock, synchronization signal and slow-control buses are provided from a custom backplane connector on the rear side of the digitizer. The Control Card has three main tasks: receives (from the preprocessing electronics) and broadcasts (to the three associated Digi-Opt12 boards) the sampling clock and synchronization signals, and performs the slow control of the associated Digi-Opt12 boards and the Control Card itself. The board is equipped with a Xilinx Spartan-6 Field Programmable Gate Array (FPGA) to fulfill

these tasks. Special care has been taken to minimize the jitter and skew of the sampling clock and synchronization signals.

Concerning the slow control, a set of synchronized registers placed in the Control Card and preprocessing FPGA have been linked to the physical slow-control buses in order to drive each device in the electronic chain from the slow control (SLC) interface. A command line interface (CLI) allows to communicate with a specific board or to broadcast signals to several back-end chains, i.e. digitizer and preprocessing electronics. The SLC has been developed around a SOAP server/client system. The SOAP server is directly running on the server hosting the preprocessing electronics, while the client could be run on any computer, thus allowing to centralize the SLC of all the GALILEO electronics on a unique place.

The communications between the digitizer module and the preprocessing electronics are performed by optical links, whereas the boards within the digitizer module are linked by means of custom communication backplane. The digitizer module is divided in two parts as each Control Card manages three Digi-Opt12 boards. The digitizer module is cooled by two fans that provide low mechanical noise, while the power consumption of the whole digitizer unit is less than 90 W for 72 digitizing channels, i.e. 1.25 W/channel.

The preprocessing board is a custom PCI express board, namely the Global Gigabit Processor (GGP), that receives digital data from the digitizer module, processes and routes them to the hosting PC by means of a 4x PCI express link. A GALILEO GGP is shown on Fig. 4. The data from 36 high-speed links at 2 Gbps are processed in a Xilinx Virtex-6 FPGA, where signal processing, timestamping and data formatting take place. Events validated by the GTS will be sent to the hosting PC via the PCI express link at a sustained rate of 400 MB/s.

After JESD204A protocol decoding, the input data are fed to an embedded First-In First-Out (FIFO) queue in order to compensate the different channel latencies. Samples then get processed in a first-level trigger generation module using fast moving window deconvolution in order to limit the influence of electronic noise and baseline fluctuations on the trigger. If the resulting signal exceeds a programmable threshold a trigger activates the energy computation mechanism and the capture of the trace, e.g. recording the trace (signal) in a time window around the triggering sample, generally set to 1 μs. The trigger module sends a trigger request to the Global Trigger and Synchronization (GTS) system, which is in charge of the synchronization of the whole array and of other detectors in the setup [34, 35].

The energy of the triggered γ ray is computed from the input pulse using a Moving Window Deconvolution (MWD) algorithm [36], tuned with a set of programmable parameters defined at the level of the slow control system. The energy computation block also includes a baseline restorer module that improves the performance of the system when working at high counting rates [37].

The 36 ADC channels of one GALILEO digitizer can be arranged within the GGP preprocessing boards depending on the connected detectors. Due to the FPGA limited dimensions, up to 27 independent triggering channels can be dealt with. Channels can be redistributed within so-called domains consisting of one master and n-slaves. The number of channels within the domains has been set as a variable parameter in the FPGA programming code, making the generation of specific firmware easier. The selection of the master trigger within the domain is a SLC parameter.

For the GASP detectors, the 36 channels are grouped in domains of 2 channels: the first acting as master trigger and the second as slave. The nine BGO crystals of each anti-Compton shield are instead grouped in a buffer box, with individually adjustable gain for each channel and up to three differential outputs. Each output can be configured to correspond to the sum of

a certain sub-set of the anti-Compton shield photo-multiplier tubes. The resulting differential signal is acquired as the slave of the surrounded HPGe detectors. In the case of the GTC, the 36 channels are organized in domains of 4 channels, where the trigger is performed on the sum of the three HPGe channels and the BGO shield signals is treated as for the GASP detectors and acquired as a slave.

Upon a trigger request, the GTS system provides a timestamp value and replies to the request within a 20 μs time window. In the typical running condition of the GALILEO array, the GTS system is used in trigger-less operation mode, meaning that all the requests are validated. The computed energy and waveforms are stored in Random Access Memory (RAM) while waiting for the validation, before being packed and sent to the PC.

The preprocessing board hosts the GTS leaf services that integrate the card within the global triggered timing system. It provides a phase-aligned 100 MHz clock to its leaves (preprocessing boards) with sub-nanosecond precision. This clock is also sent through dedicated optical links to the digitizer module with deterministic latency and hence to each ADC in the system. As discussed in the previous section, the deterministic latency is obtained by injecting a synchronization signal at the input of the ADCs, also provided synchronously by the GTS system and arriving at the digitizer module from another dedicated optical link.

4. Data Acquisition

The GALILEO DAQ is based on the XDAQ framework [38], a software suite that has been designed and developed to match the requirements of distributed data acquisition application scenarios of high-energy physics experiments. The basic unit provided by XDAQ is an executable process, which can run one or more applications.

Specific XDAQ applications are developed for the GALILEO DAQ. The XDAQ infrastructure provides data transport protocols, useful to implement the event building phase, and a set of access libraries dedicated to control custom hardware.

XDAQ executables are highly configurable through an XML configuration file, loaded at execution time. It determines the libraries to be loaded, the applications to be instantiated, the application parameters and the network connections to collaborating applications. Through this mechanism the DAQ system can be adapted to the required performance, partitioned in order to perform (test-) runs in parallel, or re-structured in case of hardware faults.

In order to handle the GALILEO data flow, multiple XDAQ applications with different functions have been developed: read-out units, filter units, builder units and merger units. All the applications are written in C++ and compiled for Scientific Linux 6 and CentOS 7 operating systems.

4.1. Read-out Units

One Read-out Unit (RUs) runs on each front-end PCs equipped with the custom preprocessing boards. A total of 4 read-out PCs are available for the GALILEO HPGe detectors, while additional 8 are fully equipped and available for the ancillary detectors. Specific read-out units have been developed for the read-out of analog VME electronics, namely the CAEN V775 and V785 TDC and ADC as for the Neutron Wall (see section 6) and digital VME electronics, namely the CAEN digitizers from the first generation namely the V1725 (250 Msps) and V1730 (500 Msps).

4.2. Local Filter Units

Local Filter units (LF) have the purpose of running dedicated algorithms on the acquired data. Different filtering can be applied, like Digital Constant Fraction Discriminator (DCFD), Pulse Shape Analysis (PSA), Compton-scattering and pile-up rejection, or other online analysis codes. At this level the events are coded in frames which consist of a five 32-bit word header, followed by up to eight 32-bit words, configurable by the users.

4.3. Builder Units

After this first level of filtering, the data frames are sent to a Builder Unit (BU) which performs the time ordering of the incoming signals and creates a complete event within a configurable time coincidence window, set to a standard value of 500 ns. Depending on the beam characteristics, i.e. continuous or pulsed beam, and physics case (prompt spectroscopy, isomeric decay, etc.). The lower limit the width of the time window is generally varied between 300 and 1000 ns. To limit the memory occupation, each Builder Units handles up to two LFs. On the GGPs, idle signals are generated to keep the triggering rate at a programmable frequency to avoid the blocking of the BUs due to missing triggers on the electronic input channels. Within a reconstructed event, the LF data frames are appended into a dedicated variable length frame with a five 32-bit word header.

4.4. Merger Unit

The Merger Unit (MU) collects and combines data from all the builder units. Additional branches, for which no builder units are requested, can be directly sent to the merger.

4.5. Global Filer Unit

Finally a Global Filter unit (GF) was implemented to perform a last stage of data filtering before storing the data on disk. In particular, the GF performs a software trigger algorithm able to select events based on the fold of the different arrays and time coincidence between GALILEO and ancillary detectors was implemented to select the events written on disk.

All DAQ applications can dump data on disk on request. Even if this feature is important in the debugging, commissioning phase, or specific experiment-dependent requirements, it may represent a bottleneck for the overall DAQ performances. In standard experiments, only the GF unit, running directly on a server connected via a dedicated Fiber Channel link to an MD3600 storage system, is writing data on disk, thus optimizing the event storing performance. In typical running conditions with a trigger rate below 20 kHz per crystal, dead time is steadily below 5%.

Servers hosting the Read-out and the Local Filter Units are located in the experimental hall, close to the detector, while the event reconstruction (BUs, MU) and event selection (GF) applications run on a host located in the laboratory computing room. The two areas are connected through a dedicated 10 Gigabit network.

All DAQ applications provide web GUIs to monitor their status. They also provide spy events on request, so that client applications can perform online analysis on a subset of acquired events, for monitoring purposes.

Figure 5 shows a simplified block diagram of the DAQ configuration. RU, BU, MU and GF are used either for GALILEO or its ancillaries, while the LF unit is dedicated to specific tasks depending on each array. The DAQ configuration is scalable to include a larger number of electronic channels for HPGe detectors or other GALILEO ancillaries.

5. GALILEO Array Performances

In this section, the performances of the array, in terms of P/T and γ-ray detection efficiency, are presented. Detailed Monte-Carlo simulations, performed with the GEANT4 toolkit [39] and the AGATA simulation package [40] will be discussed. Complete simulation of the GALILEO array and its ancillaries have shown to be helpful for the analysis of the performed experiments [8].

5.1. Efficiency

As it is shown in Fig. 6, and commented in section 2, the gain in efficiency between Phase I and Phase II is about a factor 2, owing to the addition of GTC detectors. The absolute full-energy peak efficiency for GALILEO Phase II is 4.1% for 1.3 MeV γ rays before add-back in the triple cluster. Including the add-back, a 20% increase in photo-peak efficiency for the triple cluster is obtained allowing to reach a 4.5% total efficiency at 1.3 MeV. From the comparison with the experimental data measured with standard γ-ray sources (^{152}Eu, ^{137}Cs, ^{60}Co, ^{88}Y), the simulation describes well the performances of the array at energy above 200 keV. Discrepancies between the simulated and measured photo-peak efficiency are observed at low energies, mostly arising from the fact that the charge collection is not included in the simulation, thus not reproducing the known inhomogeneity of the electric field on the first layers of the crystal.

5.2. Peak-to-total and Compton-Rejection

To reject Compton-scattering events, GALILEO detectors are equipped with BGO anti-Compton shields. As discussed in the description of the mechanics of GALILEO, Pb shielding and Hevimet collimators are implemented in the structure to avoid direct interaction of the γ rays in the BGO shield.

In order to improve the P/T ratio, the Compton-scattering rejection for the GALILEO array is performed in two steps. In a first stage, the events in time coincidence (100 ns) between BGO and HPGe detectors are discarded at LF level, allowing to reduce the data bandwidth on the acquisition system. For all the remaining events, time and energy information of the BGO-shield are written to disk and an additional condition can be applied by the user to optimize the P/T keeping the efficiency under control. Results of the Compton suppression procedure are shown in Fig. 7, where a spectrum before and after Compton-scattering rejection is presented, together with the scattered γ rays. The measured P/T using a ^{60}Co source for the tapered crystal lies in the range between 55-60%. For the triple cluster, including the add-back procedure a P/T of 45-50% is obtained. Fig. 8 shows the evolution of the P/T ratio of the tapered crystal as a function of the energy. To better reproduce experimental data, light threshold detection on the AC shield can be adjusted.

6. Ancillaries

Ancillary detectors are essential instruments in γ-ray spectroscopy studies, allowing the investigation of specific reaction channels. GALILEO can be coupled to a continuously increasing variety of complementary instrumentation to detect both light-charged particles and heavy ions, neutrons and high-energy γ rays.

The signals from ancillary detectors are generally processed through the back-end and DAQ infrastructure of the GALILEO array. This implies that wave-forms are digitized with 100 MHz sampling rate and 14-bit conversion precision. At need, the custom GALILEO digitizers can be

replaced by commercial ones, synchronized and timestamped using the GTS system described in Sec. 4. The information obtained by numerical treatment of the digital samples, for example time and energy values, are then sent to the data acquisition framework based on XDAQ architecture.

Valuable information can be obtained when high resolution γ-ray spectra are measured in coincidence with high-energy γ-rays, light-charged particles, high heavy ions and/or neutrons. In Coulomb excitation reactions for example, the detection of heavy-ions is necessary to reconstruct the kinematics and extract cross-sections of the excited states of interest.

In fusion-evaporation reactions, detection of the emitted particles and/or of the evaporation residue (ER) detection allows to largely improve the γ-ray spectra and extract structure properties of the nuclei of interest.

6.1. High-energy γ rays

When the number of the states populated in a reaction is limited, e.g. when studying light nuclei or even-even nuclei in proximity of the shell closures, or in the case of studies of high-lying resonant states (Giant Resonances), the resolution of the γ-ray detectors might not be the primary asset, while it is crucial to maximize the detection efficiency.

Ten $LaBr_3$:Ce detectors (3"×3") [12] can be added to the GALILEO HPGe detectors to this scope, at a distance varying between ∼120 mm to ∼200 mm with respect to the target position, and at 70° with respect to the beam line. When placed at 200 mm from the target position, the $LaBr_3$:Ce array has a full-energy peak efficiency of 2.3% at 1.3 MeV, and a simulated efficiency of ∼0.8% at 16 MeV. The 3D rendering of $LaBr_3$:Ce (depicted in red) detectors in GALILEO Phase I, located at 70° is shown in Fig. 9. The $LaBr_3$:Ce array can also replace HPGe detectors on the 90° ring.

The implementation of the fast signals coming from the $LaBr_3$:Ce detectors into the DAQ of GALILEO was compared to a standard analog chain. The fast signals coming from the $LaBr_3$:Ce detectors are formed by the custom-designed module LaBr-PRO [41]. For each detector, this module provides a logic signal corresponding to the zero-crossing of the CFD and two energy signals (fast and slow integration). Since the pulse shape analysis is not of interest for our applications, the choice was made to send to the digitizers the CFD and energy signal corresponding to the slow integration. Triggering on the logic signals and performing a digital CFD on these logical signals, a time resolution of ≈850 ps was obtained at the ^{60}Co. This was compared to the time resolution obtained by sending the same CFD signals to TAC (Time to Amplitude Converter) modules and then digitizing the output of the TACs, obtaining similar performances, ≈700 ps. It is worth pointing out that the detectors used in this case are not optimized in any way for fast-timing measurement. Similar performances to a standard analog chain have been registered also with respect to the energy resolution, of about 3% at 661.6 keV for both digitized signals.

To further improve the performances of these detectors and their applications, a read-out using commercial digitizers, provided by CAEN, with sampling frequency up to 500 Msps was implemented. The read-out is fully integrated in the XDAQ acquisition and allows the complete coupling to the GALILEO array. A 100 MHz Low-Voltage Differential Signal (LVDS) clock signal is sent from the VME GTS-carrier directly into the CAEN digitizers assuring the clocks synchronization of the two systems. Since the CAEN clock counter (timestamp) is reset at each start and stop of the DAQ, while the GTS clock counters is programmed to go around a 48-bit value, a determination of the offset between the two system is necessary. The AGAVA module [26], developed to couple VME read-out with the AGATA infrastructure, is used to perform this operation. The logic signal used to start the commercial boards is sent to the trigger-in of

the AGAVA board, allowing to determine the GTS t_0 timestamp. Fluctuations of the offset of ± 1 clock cycle over the different start/stop cycles have been observed but can be corrected offline. The automatic determination of the offset between the two read-outs, allows to fully integrate the CAEN electronics in the XDAQ acquisition chain. Using this dedicated digital electronic read-out both energy and time resolution are equal to what can be obtained using dedicated analog read-out. This read-out was also tested with fast-responding scintillators, e.g. PARIS [42, 43] and FATIMA [44, 45] for which time resolution of ∼250 ps is obtained using the V1730 digitizers [46].

6.2. Light-charged particles

Light charged particle-detector arrays ($Z \leq 6$) are used with GALILEO in two different configurations: large angular coverage, on one side, and high energy and angular resolution, on the other. The two particle arrays available for GALILEO are EUCLIDES and GALTRACE, described in the following and represented in Fig. 11. EUCLIDES is designed to enhance the channel selection in fusion-evaporation experiment. The high granularity and resolution of GALTRACE, on the contrary, is exploited for direct-reaction spectroscopic studies.

- EUCLIDES is a 4π light-charged particle detector, made up of 40 two-stage ΔE-E telescopes, arranged in a 42-faces polyhedron composed of 30 irregular hexagonal and 12 regular pentagonal faces. The forward-most part is composed of 5 hexagonal telescopes electrically segmented in 4 sectors with equal geometrical areas.

  The geometrical efficiency of the array is about 81%. The total efficiency for the full EUCLIDES array was derived using the average experimental values, assuming an isotropic distribution of the emitted particles and neglecting the probability of multiple hits in each detector. It accounts to 60% and 40%, for protons and alpha particles, respectively. The design, characteristics and performance of the EUCLIDES array are presented and discussed in a dedicated paper [6].

- GALTRACE is a highly-segmented silicon detector for light particles and ions [7]. It consists of a series of silicon layers in ΔE-E telescope configuration, whose thickness is 200 μm and 1.5 mm, respectively. Each detector, 50x20 mm^2 in size, is segmented in 60 pads, 4x4 mm^2 each, in order to achieve an angular resolution of few degrees when the detector is placed at a distance $\gtrsim$ 50 mm from the target position. GALTRACE is equipped with integrated preamplifiers developed by the INFN electronics group of Milano [47]. The ASIC preamplifiers have 8 anodic channels each, plus one cathodic channel. The cathode is powered separately and can be shut off if not used. The cathodic channel is used as trigger. The read-out of one complete ΔE-E telescope requires 64 preamplifier anodic channels and 2 cathodic channels, therefore making use of 8 ASIC preamplifiers. The preamplifier board makes use of a fast-reset circuit similar to the one employed on the GALILEO preamplifier boards. The signals are transported out of the reaction chamber in single-ended mode. A short connection to the single-ended to differential (SeDiff) modules allows for long connections to the GALILEO digitizers in the back-end. These boards are compliant with preamplifier standards in terms of dynamic range, bandwidth and noise. The quality of preamplifiers and the short connections entail the possible use of pulse-shape analysis [48, 49] to resolve the reaction channel.

Array	Detection	$\delta\theta$ [°]	$\Omega/4\pi$ [%]	Efficiency [%]
EUCLIDES	p, α	2.5÷5	81	60 (p), 40 (α)
SPIDER	HI	1.5÷3	20.2	~17
GALTRACE	p, α, LI	~2	~20	~18
$LaBr_3$:Ce	high-E γ rays	~10		2.2
Neutron Wall	n	10	25	20 (1n), 1 (2n)
RFD	HI	0.1	~0.1	20÷50

Table 2: Main characteristics of GALILEO complementary instrumentation in terms of radiation detection, angular resolution, geometrical and absolute efficiency. See section 6 for further details.

6.3. Heavy ions

As for light-charged particles, GALILEO can be coupled to two different heavy ion detectors: covering the backward hemishpere with the SPIDER Si-detector array and forward angles with the RFD array.

- SPIDER [8] (Silicon PIe DEtectoR) is an array of segmented silicon detectors developed by INFN Firenze in collaboration with INFN LNL, INFN Padova and INFN Milano for low-energy Coulomb excitation measurements. It is composed of trapezoidal silicon detectors (300 μm thick) segmented in 8 independent strips. The array provides excellent energy resolution (0.5% for α-particles at 5.5 MeV). This permits to account for the energy losses in the target and derive its thickness [50] via the optimization of the Doppler correction of the γ-ray spectra. Such information is essential in Coulomb excitation experiments with stable beams to derive the absolute cross section.

  When coupled with GALILEO, SPIDER is shaped into a cone-like configuration composed of 7 detectors positioned at a distance of about 85 mm from the target (see Fig. 11 right-most panel).

  In this configuration, the array angular coverage is 17% of 4π (total solid angle). The polar angle coverage is from 124 to 161 degrees with respect to the beam direction. A 3D-printed aluminium holder allows for an easy mounting of SPIDER in the GALILEO vacuum chamber, and a dedicated PCB interfaces the array with the same FEE/BEE of EUCLIDES. At present, SPIDER is employed for experiments with stable beams [51]. It is mounted at backward angles to limit the radiation damage and to enhance the probability of multi-step Coulomb excitation and the sensitivity to second-order effects. In the near future, low-energy Coulomb excitation studies will greatly benefit from the radioactive beams provided by SPES. For these experiments, SPIDER will be mounted at forward angles to compensate for the low intensity of the ISOL beams.

- RFD [52] consists of 18 fast scintillators distributed around the beam axis. They detect electrons stripped as ion cross a mylar foil placed in front of each detector. RFD detects forward focused recoils, measures their time of flight and position angle in event-by-event mode, thus providing a velocity vector for a single ER. The γ-recoil time coincidence condition and the selection of the ToF range, which is specific for ER, allows to suppress γ-rays from competing reaction channels, such as fission and transfer processes, Coulomb excitation, and disentangling possible products coming from target contamination, etc.

Typical ER detection efficiency of RFD is 20-50% and depends on the reaction kinematics. It can be optimized by adjusting the flight distance from the target.

In order to limit the counting rate, which can easily reach MHz, signals of the RFD have to be vetoed using the radio-frequency signals delivered by the XTU Tandem bunching system. The vetoed signals from the RFD detectors are fed to the MegAmp NIM modules developed by INFN Milano [53]. Each module can host up to 16 channels and give an energy signal and a TAC signal providing a common external stop signal. The output of the MegAmp amplifier is then fed into the Single-Ended-to-differential modules developed for the GALTRACE array to be transported to the GALILEO digitizers.

The mechanical coupling of RFD to GALILEO is shown in the 3D rendering reported in Fig. 10.

6.4. Neutrons

Neutron Wall [9] is an array of organic Bicron BC501A liquid scintillators. The array consists of 15 hexagonal detectors (H) and 1 pentagonal detector (P). H detectors present 3 segments per unit, each one filled with 3.2 liters of liquid scintillator. The P detector is composed by 5 segments, 1.1 liters each. In the GALILEO configuration, there is a total of 45 detector segments for a volume of liquid scintillator of about 150 liters.

The detectors are mounted in a closely packed configuration forming a pseudo-spherical shell that covers about 30% of 4π solid angle. Neutron Wall is mounted in the forward hemisphere, with GALILEO detectors occupying the backward hemisphere, as shown in the top panel of Fig. 9. The distance from the target to the front face of the detectors is about 500 mm. Measured efficiency is 20% and 1% for 1n an 2n detection, respectively.

In the future the use of Neutron Wall and NEDA [54] in combination with GALILEO is also envisaged.

6.5. Lifetime and electromagnetic moment measurements

Lifetime and electromagnetic moments provide a stringent test of nuclear models. High precision measurements are of key importance in the understanding of nuclear forces, in particular for the role of isospin mixing or quadrupole-pairing interplay. In order to get access to level lifetimes in the range of the fs to the ns, the GALILEO array can be coupled to several ancillaries.

A dedicated plunger device has been developed in collaboration with the IKP (Cologne) [10] to cover the ps to the ns range.

The possibility of performing fast-timing measurements with the inclusion of a number of the fast-responding $LaBr_3$:Ce detectors of the FATIMA collaboration is also made available. The integration of these detectors has been discussed before in this section.

7. Conclusions

The GALILEO γ-ray spectrometer has been developed and it is presently installed at the Legnaro National Laboratories, INFN. In the final phase, it consists of 55 HPGe detectors: 10 triple clusters and 25 single crystals, arranged in 6 rings at 150°, 116°, 90°, 61°, 51°and 28°with respect to the beam optical axis.

The read out chain is composed by differential charge-sensitive fast-reset preamplifiers, digitizers boards and preprocessing cards which receive digital data and route them to the hosting computers.

The data acquisition system of the GALILEO array is based on XDAQ platform developed at CERN for distributed acquisition system.

The GALILEO spectrometer can be assisted by a variety of complementary instrumentation to detect light-charged particles and ions, neutrons, high-energy γ rays and measure electromagnetic moments.

The array has been successfully commissioned and is under operation running scientific campaigns to investigate neutron-deficient and neutron-rich nuclei in various regions of the Segré chart, using stable and, in the near future, radioactive beams from the SPES facility.

8. Acknowledgments

The research leading to these results has received funding from the European Union HORIZON2020 research and innovation programme under Grant Agreement n 654002 - ENSAR2.

Authors are grateful to the GAMMAPOOL European Gamma-Ray Spectroscopy Pool for the loan of the EUROBALL clusters and their anti-Compton shields, the EUCLIDES Si-ball, and the NeutronWall detectors. Authors acknowledge the contribution of the RFD collaboration, the IKP Cologne Plunger group, and the support of L. M. Fraile and J.-M. Régis for the fast timing $LaBr_3$:Ce array. A. Goasduff is grateful to the support of Fondazione Cassa di Risparmio Padova e Rovigo. The activity of A. Gadea is financed by Ministerio de Ciencia e Innovación and Generalitat Valenciana, Spain, under the Grants SEV-2014-0398, FPA2017-84756-C4, PROMETEO/2019/005 and by the EU FEDER funds. G. Jaworski is grateful for the supported by the National Science Centre, Poland (NCN) (grant No. 2017/25/B/ST2/01569). M. Siciliano is grateful to the support of the U.S. Department of Energy, Office of Science, Office of Nuclear Physics, under contract number DE-AC02-06CH11357. F.C.L. Crespi, A. Goasduff, A. Gottardo and F. Recchia acknowledge the support from the MIUR PRIN 2017 call for funding, project 2017P8KMFT. The authors would like to thank the operators of the LNL Tandem-Alpi-Piave accelerator complex and the target laboratory for the excellent beams provided and the quality of the targets. CloudVeneto [55] is acknowledged for the use of computing and storage facilities.

9. Bibliography

References

[1] C. A. Ur, The tandem-alpi-piave accelerator complex of lnl, AIP Conference Proceedings 1530 (1) (2013) 35. doi:10.1063/1.4812903.

[2] T. Marchi, G. Prete, F. Gramegna, A. Andrighetto, P. Antonini, M. Ballan, M. Bellato, L. Bellan, D. Benini, G. Bisoffi, J. Bermudez, G. Benzoni, D. Bortolato, F. Borgna, A. Calore, S. Canella, S. Carturan, N. Ciatara, M. Cinausero, P. Cocconi, A. Cogo, D. Conventi, V. Conte, M. Comunian, L. Costa, S. Corradetti, G. de Angelis, C. de Martinis, P. D. Ruvo, J. Esposito, E. Fagotti, D. Fabris, P. Favaron, E. Fioretto, A. Galatá, F. Gelain, M. Giacchini, D. Giora, A. Gottardo, M. Gulmini, M. Lollo, A. Lombardi, M. Manzolaro, M. Maggiore, D. Maniero, P. F. Mastinu, A. Monetti, F. Pasquato, R. Pegoraro, A. Pisent, M. Poggi, S. Pavinato, L. Pranovi, D. Pedretti, C. Roncolato, M. Rossignoli, L. Sarchiapone, D. Scarpa, J. J. Valiente-Dobón, V. Volpe, A. Vescovo, D. Zafiropoulos, The SPES facility at legnaro national laboratories, Journal of Physics: Conference Series 1643 (2020) 012036. doi:10.1088/1742-6596/1643/1/012036.

[3] D. Bazzacco, Proc. int. conf. on nuclear structure at high angular momentum, Proceedings AECL 10613 2 (1992).

[4] F. Beck, Euroball: Large gamma ray spectrometers through european collaborations, Progress in Particle and Nuclear Physics 28 (1992) 443. doi:https://doi.org/10.1016/0146-6410(92)90047-6.

[5] C. W. Beausang, J. Simpson, Large arrays of escape suppressed spectrometers for nuclear structure experiments, JPG 22 (5) (1996) 527–558. doi:10.1088/0954-3899/22/5/003.

[6] D. Testov, D. Mengoni, A. Goasduff, A. Gadea, R. Isocrate, P. R. John, G. de Angelis, D. Bazzacco, C. Boiano, A. Boso, P. Cocconi, J. Dueñas, F. J. Egea Canet, L. Grassi, K. Hadyńska-Klęk, G. Jaworski, S. Lunardi, R. Menegazzo, D. R. Napoli, F. Recchia, M. Siciliano, J. J. Valiente-Dobón, The 4π highly-efficient light-charged-particle detector euclides, installed at the galileo array for in-beam γ-ray spectroscopy, Eur. Phys. J. A 55 (4) (2019) 47. doi:10.1140/epja/i2019-12714-6.

[7] D. Mengoni, Trace: a highly-segmented silicon detector for light charged particles emitted in fusion-evaporation and direct nuclear reactions, Ph.D. thesis, Univ. of Camerino, Italy (2008).

[8] M. Rocchini, K. Hadyńska-Klęk, A. Nannini, J. Valiente-Dobón, A. Goasduff, D. Testov, D. Mengoni, P. John, M. Siciliano, B. Melon, P. Sona, M. Ottanelli, A. Perego, M. Chiari, M. Zielińska, D. Bazzacco, G. Benzoni, S. Bettarini, M. Brianzi, F. Camera, P. Cocconi, C. Czelusniak, D. Doherty, M. Komorowska, N. Marchini, M. Matejska-Minda, P. Napiorkowski, E. Pasquali, L. Ramina, M. Rampazzo, F. Recchia, D. Rosso, L. Sottili, A. Tredici, Spider: A silicon pie detector for low-energy coulomb-excitation measurements, Nucl. Instrum. Methods A 971 (2020) 164030. doi:https://doi.org/10.1016/j.nima.2020.164030.

[9] O. Skeppstedt, H. Roth, L. Lindström, R. Wadsworth, I. Hibbert, N. Kelsall, D. Jenkins, H. Grawe, M. Górska, M. Moszyǹski, Z. Sujkowski, D. Wolski, M. Kapusta, M. Hellström, S. Kalogeropoulos, D. Oner, A. Johnson, J. Cederkäll, W. Klamra, J. Nyberg, M. Weiszflog, J. Kay, R. Griffiths, J. G. Narro, C. Pearson, J. Eberth, The euroball neutron wall - design and performance tests of neutron detectors, Nucl. Instrum. Methods A 421 (1999) 531 – 541. doi:https://doi.org/10.1016/S0168-9002(98)01208-X.

[10] C. Müller-Gatermann, F. von Spee, A. Goasduff, D. Bazzacco, M. Beckers, T. Braunroth, A. Boso, P. Cocconi, G. de Angelis, A. Dewald, C. Fransen, A. Goldkuhle, A. Gottardo, A. Gozzelino, K. Hadyńska-Klęk, G. Jawroski, P. R. John, J. Jolie, S. M. Lenzi, J. Litzinger, R. Menegazzo, D. Mengoni, D. R. Napoli, F. Recchia, M. Siciliano, D. Testov, S. Thiel, J. J. Valiente-Dobón, K. O. Zell, A new dedicated plunger device for the galileo γ-ray detector array, Nucl. Instrum. Methods A 920 (2019) 95 – 99. doi:https://doi.org/10.1016/j.nima.2018.12.077.

[11] J. Bradbury, D. Testov, S. Bakes, A. Goasduff, D. Mengoni, J. Valiente-Dobón, G. de Angelis, D. Bazzacco, C. Boiano, A. Boso, B. Cederwall, M. Cicerchia, G. Colucci, P. Čolović, F. Didierjean, M. Doncel, J. Duenas, F. Galtarossa, A. Gozzelino, K. Hadyńska-Klęk, G. Jaworski, P. John, H. Liu, S. Lenzi, S. Lunardi, R. Menegazzo, A. Mentana, C. Müller-Gatermann, D. Napoli, G. Pasqualato, F. Recchia, M. Rocchini, S. Riccetto, B. Saygi, M. Siciliano, Y. Sobolev, S. Szilner, Lifetime measurements using a plunger device and the euclides si array at the galileo γ-ray spectrometer, Nuclear Instruments and Methods in Physics Research Section A: Accelerators, Spectrometers, Detectors and Associated Equipment 979 (2020) 164345. doi:https://doi.org/10.1016/j.nima.2020.164345.

[12] A. Giaz, L. Pellegri, S. Riboldi, F. Camera, N. Blasi, C. Boiano, A. Bracco, S. Brambilla, S. Ceruti, S. Coelli, F. Crespi, M. Csatlòs, S. Frega, J. Gulyàs, A. Krasznahorkay, S. Lodetti, B. Million, A. Owens, F. Quarati, L. Stuhl, O. Wieland, Characterization of large volume 3.5″×8″ LaBr3:Ce detectors, Nucl. Instrum. Methods A 729 (2013) 910 – 921. doi:https://doi.org/10.1016/j.nima.2013.07.084.

[13] G. L. Zhang, G. X. Zhang, S. P. Hu, Y. J. Yao, J. B. Xiang, H. Q. Zhang, J. Lubian, J. L. Ferreira, B. Paes, E. N. Cardozo, H. B. Sun, J. J. Valiente-Dobón, D. Testov, A. Goasduff, P. R. John, M. Siciliano, F. Galtarossa, R. Francesco, D. Mengoni, D. Bazzacco, E. T. Li, X. Hao, W. W. Qu, One-neutron stripping processes to excited states of ^{90}Y* in the ^{89}Y(^{6}Li,^{5} Li)^{90}Y* reaction, Phys. Rev. C 97 (2018) 014611.

[14] Y. H. Qiang, C. M. Petrache, S. Guo, P. M. Walker, D. Mengoni, Q. B. Chen, B. F. Lv, A. Astier, E. Dupont, M. L. Liu, X. H. Zhou, J. G. Wang, D. Bazzacco, A. Boso, A. Goasduff, F. Recchia, D. Testov, F. Galtarossa, G. Jaworski, D. R. Napoli, S. Riccetto, M. Siciliano, J. J. Valiente-Dobon, C. Andreoiu, F. H. Garcia, K. Ortner, K. Whitmore, B. Cederwall, E. A. Lawrie, I. Kuti, D. Sohler, T. Marchlewski, J. Srebrny, A. Tucholski, A. C. Dai, F. R. Xu, Identification of high-k rotation in ^{130}Ba: Testing the consistency of electromagnetic observables, Phys. Rev. C 99 (2019) 014307.

[15] C. Petrache, P. Walker, S. Guo, Q. Chen, S. Frauendorf, Y. Liu, R. Wyss, D. Mengoni, Y. Qiang, A. Astier, E. Dupont, R. Li, B. Lv, K. Zheng, D. Bazzacco, A. Boso, A. Goasduff, F. Recchia, D. Testov, F. Galtarossa, G. Jaworski, D. Napoli, S. Riccetto, M. Siciliano, J. Valiente-Dobon, M. Liu, X. Zhou, J. Wang, C. Andreoiu, F. Garcia, K. Ortner, K. Whitmore, T. Bck, B. Cederwall, E. Lawrie, I. Kuti, D. Sohler, J. Timr, T. Marchlewski, J. Srebrny, A. Tucholski, Diversity of shapes and rotations in the γ-soft ^{130}ba nucleus: First observation of a t-band in the $a = 130$ mass region, Phys. Lett. B 795 (2019) 241.

[16] Y.-F. Lv, J.-B. Lu, G.-L. Zhang, Y.-H. Wu, C.-X. Yuan, G.-J. Fu, G.-X. Zhang, Z. Huang, M.-L. Wang, S.-P. Hu, H.-B. Sun, H.-Q. Zhang, C.-Q. Li, K.-Y. Ma, Y.-J. Ma, Y.-Z. Liu, D. Testov, P. R. John, J. J. Valiente-Dobon, A. Goasduff, M. Siciliano, F. Galtarossa, F. Recchia, D. Mengoni, D. Bazzacco, Low-lying states of ^{92,93}Nb excited in the reactions induced by the weakly-bound nucleus ^{6}Li near the coulomb barrier, Chinese Physics C 43 (10) (2019) 104102.

[17] N. Marchini, M. Rocchini, A. Nannini, D. T. Doherty, M. Zielińska, P. E. Garrett, K. Hadyńska-Klęk, D. Testov, A. Goasduff, G. Benzoni, F. Camera, S. D. Bakes, D. Bazzacco, A. Bergmaier, T. Berry, H. Bidaman, V. Bildstein, D. Brugnara, V. H. Brunet, W. N. Catford, M. De Rizzo, A. Diaz Varela, T. Fäestermann, F. Galtarossa, N. Gelli, A. Gottardo, A. Gozzellino, R. Hertenberger, Illana, A., J. Keatings, A. R. Kennington, D. Mengoni, L. Morrison,

D. R. Napoli, M. Ottanelli, G. Pasqualato, F. Recchia, S. Riccetto, M. Scheck, M. Siciliano, G. Sighinolfi, J. Sinclair, P. Spagnoletti, J. J. Valiente Dobón, M. Vandebrouck, K. Wrzosek-Lipska, I. Zanon, Shape coexistence in ^{94}Zr studied via coulomb excitation, EPJ Web Conf. 223 (2019) 01038. doi:10.1051/epjconf/201922301038.

[18] S. Guo, C. Petrache, D. Mengoni, Y. Qiang, Y. Wang, Y. Wang, J. Meng, Y. Wang, S. Zhang, P. Zhao, A. Astier, J. Wang, H. Fan, E. Dupont, B. Lv, D. Bazzacco, A. Boso, A. Goasduff, F. Recchia, D. Testov, F. Galtarossa, G. Jaworski, D. Napoli, S. Riccetto, M. Siciliano, J. Valiente-Dobon, M. Liu, G. Li, X. Zhou, Y. Zhang, C. Andreoiu, F. Garcia, K. Ortner, K. Whitmore, A. Ata-Nyberg, T. Bck, B. Cederwall, E. Lawrie, I. Kuti, D. Sohler, T. Marchlewski, J. Srebrny, A. Tucholski, Evidence for pseudospin-chiral quartet bands in the presence of octupole correlations, Phys. Lett. B 807 (2020) 135572. doi:https://doi.org/10.1016/j.physletb.2020.135572.

[19] S. Guo, C. M. Petrache, D. Mengoni, Y. X. Liu, Q. B. Chen, Y. H. Qiang, A. Astier, E. Dupont, K. K. Zheng, J. G. Wang, B. Ding, B. F. Lv, M. L. Liu, Y. D. Fang, X. H. Zhou, D. Bazzacco, A. Boso, A. Goasduff, F. Recchia, D. Testov, F. Galtarossa, G. Jaworski, D. R. Napoli, S. Riccetto, M. Siciliano, J. J. Valiente-Dobon, C. Andreoiu, F. H. Garcia, K. Ortner, K. Whitmore, B. Cederwall, E. A. Lawrie, I. Kuti, D. Sohler, T. Marchlewski, J. Srebrny, A. Tucholski, Pseudospin partner bands in ^{130}Ba, Phys. Rev. C 102 (2020) 044320. doi:10.1103/PhysRevC.102.044320.

[20] M. Siciliano, I. Zanon, A. Goasduff, P. R. John, T. R. Rodríguez, S. Péru, I. Deloncle, J. Libert, M. Zielińska, D. Ashad, D. Bazzacco, G. Benzoni, B. Birkenbach, A. Boso, T. Braunroth, M. Cicerchia, N. Cieplicka-Oryńczak, G. Colucci, F. Davide, G. de Angelis, B. de Canditiis, A. Gadea, L. P. Gaffney, F. Galtarossa, A. Gozzelino, K. Hadyńska-Klęk, G. Jaworski, P. Koseoglou, S. M. Lenzi, B. Melon, R. Menegazzo, D. Mengoni, A. Nannini, D. R. Napoli, J. Pakarinen, D. Quero, P. Rath, F. Recchia, M. Rocchini, D. Testov, J. J. Valiente-Dobón, A. Vogt, J. Wiederhold, W. Witt, Shape coexistence in neutron-deficient ^{188}Hg investigated via lifetime measurements, Phys. Rev. C 102 (2020) 014318. doi:10.1103/PhysRevC.102.014318.

[21] C. B. Li, G. L. Zhang, C. X. Yuan, G. X. Zhang, S. P. Hu, W. W. Qu, Y. Zheng, H. Q. Zhang, D. Mengoni, D. Testov, J. J. Valiente-Dobón, H. B. Sun, N. Wang, X. G. Wu, G. S. Li, M. Mazzocco, A. Gozzelino, C. Parascandolo, D. Pierroutsakou, M. La Commara, F. Recchia, A. I. Sison, S. Bakes, I. Zanon, S. Aydin, D. Bazzacco, New level scheme and shell model description of ^{212}Rn, Phys. Rev. C 101 (2020) 044313. doi:10.1103/PhysRevC.101.044313.

[22] M. Rocchini, K. Hadyńska-Klęk, A. Nannini, A. Goasduff, M. Zielińska, D. Testov, T. R. Rodríguez, A. Gargano, F. Nowacki, G. De Gregorio, H. Naïdja, P. Sona, J. J. Valiente-Dobón, D. Mengoni, P. R. John, D. Bazzacco, G. Benzoni, A. Boso, P. Cocconi, M. Chiari, D. T. Doherty, F. Galtarossa, G. Jaworski, M. Komorowska, N. Marchini, M. Matejska-Minda, B. Melon, R. Menegazzo, P. J. Napiorkowski, D. Napoli, M. Ottanelli, A. Perego, L. Ramina, M. Rampazzo, F. Recchia, S. Riccetto, D. Rosso, M. Siciliano, Onset of triaxial deformation in ^{66}Zn and properties of its first excited 0^+ state studied by means of coulomb excitation, Phys. Rev. C 103 (2021) 014311. doi:10.1103/PhysRevC.103.014311.

[23] D. A. Testov, A. Boso, S. M. Lenzi, F. Nowacki, F. Recchia, G. de Angelis, D. Bazzacco, G. Colucci, M. Cottini, F. Galtarossa, A. Goasduff, A. Gozzelino, K. Hadyńska-Klęk, G. Jaworski, P. R. John, S. Lunardi, R. Menegazzo, D. Mengoni, A. Mentana, V. Modamio, A. Nannini, D. R. Napoli, M. Palacz, M. Rocchini, M. Siciliano, J. J. Valiente-Dobón, High-spin intruder states in the mirror nuclei ^{31}S and ^{31}P, Phys. Rev. C 104 (2021) 024309. doi:10.1103/PhysRevC.104.024309.
URL `https://link.aps.org/doi/10.1103/PhysRevC.104.024309`

[24] D. A. Testov, S. Bakes, J. J. Valiente-Dobón, A. Goasduff, S. Frauendorf, F. Nowacki, T. R. Rodríguez, G. de Angelis, D. Bazzacco, C. Boiano, A. Boso, B. Cederwall, M. Cicerchia, P. Čolović, G. Colucci, F. Didierjean, M. Doncel, J. A. Dueñas, F. Galtarossa, A. Gozzelino, K. Hadyńska-Klęk, G. Jaworski, P. R. John, S. Lenzi, H. Liu, S. Lunardi, R. Menegazzo, D. Mengoni, A. Mentana, D. R. Napoli, G. Pasqualato, F. Recchia, S. Riccetto, L. M. Robledo, M. Rocchini, B. Saygi, M. Siciliano, Y. Sobolev, S. Szilner, Octupole correlations near ^{110}Te, Phys. Rev. C 103 (2021) 044321. doi:10.1103/PhysRevC.103.044321.

[25] G. Gosta, A. Mentana, F. Camera, A. Bracco, S. Ceruti, G. Benzoni, N. Blasi, S. Brambilla, S. Capra, F. C. L. Crespi, A. Giaz, S. Leoni, B. Million, S. Riboldi, C. Porzio, S. Ziliani, O. Wieland, A. Nannini, M. Rocchini, N. Marchini, M. Ciemała, M. Kmiecik, A. Maj, B. Wasilewska, M. Zieblinski, D. Filipescu, J. Kaur, N. Marginean, S. Pascu, T. Glodariu, D. Ghita, V. Zamfir, J. J. Valiente-Dobón, G. de Angelis, F. Galtarossa, A. Goasduff, T. Bayram, A. Gadea, A. Montaner, I. Zanon, D. Brugnara, A. Gozzelino, G. Pasqualato, R. Menegazzo, A. Gottardo, G. Jaworski, S. Lenzi, D. Napoli, D. Testov, M. Siciliano, T. Marchi, D. Mengoni, D. Bazzacco, A. Boso, P. R. John, F. Recchia, R. Raabe, O. Poleshchuk, J. Yang, Probing isospin mixing with the giant dipole resonance in the ^{60}Zn compound nucleus, Phys. Rev. C 103 (2021) L041302. doi:10.1103/PhysRevC.103.L041302.

[26] S. Akkoyun, A. Algora, B. Alikhani, F. Ameil, G. de Angelis, L. Arnold, A. Astier, A. Ataç, Y. Aubert, C. Aufranc, A. Austin, S. Aydin, F. Azaiez, S. Badoer, D. Balabanski, D. Barrientos, G. Baulieu, R. Baumann, D. Bazzacco, F. Beck, T. Beck, P. Bednarczyk, M. Bellato, M. Bentley, G. Benzoni, R. Berthier, L. Berti, R. Beunard, G. L. Bianco, B. Birkenbach, P. Bizzeti, A. Bizzeti-Sona, F. L. Blanc, J. Blasco, N. Blasi, D. Bloor, C. Boiano, M. Borsato, D. Bortolato, A. Boston, H. Boston, P. Bourgault, P. Boutachkov, A. Bouty, A. Bracco, S. Brambilla, I. Brawn,

A. Brondi, S. Broussard, B. Bruyneel, D. Bucurescu, I. Burrows, A. Bürger, S. Cabaret, B. Cahan, E. Calore, F. Camera, A. Capsoni, F. Carri, G. Casati, M. Castoldi, B. Cederwall, J.-L. Cercus, V. Chambert, M. E. Chambit, R. Chapman, L. Charles, J. Chavas, E. Clment, P. Cocconi, S. Coelli, P. Coleman-Smith, A. Colombo, S. Colosimo, C. Commeaux, D. Conventi, R. Cooper, A. Corsi, A. Cortesi, L. Costa, F. Crespi, J. Cresswell, D. Cullen, D. Curien, A. Czermak, D. Delbourg, R. Depalo, T. Descombes, P. Désesquelles, P. Detistov, C. Diarra, F. Didierjean, M. Dimmock, Q. Doan, C. Domingo-Pardo, M. Doncel, F. Dorangeville, N. Dosme, Y. Drouen, G. Duchêne, B. Dulny, J. Eberth, P. Edelbruck, J. Egea, T. Engert, M. Erduran, S. Ertürk, C. Fanin, S. Fantinel, E. Farnea, T. Faul, M. Filliger, F. Filmer, C. Finck, G. de France, A. Gadea, W. Gast, A. Geraci, J. Gerl, R. Gernhäuser, A. Giannatiempo, A. Giaz, L. Gibelin, A. Givechev, N. Goel, V. González, A. Gottardo, X. Grave, J. Grębosz, R. Griffiths, A. Grint, P. Gros, L. Guevara, M. Gulmini, A. Görgen, H. Ha, T. Habermann, L. Harkness, H. Harroch, K. Hauschild, C. He, A. Hernández-Prieto, B. Hervieu, H. Hess, T. Hÿük, E. Ince, R. Isocrate, G. Jaworski, A. Johnson, J. Jolie, P. Jones, B. Jonson, P. Joshi, D. Judson, A. Jungclaus, M. Kaci, N. Karkour, M. Karolak, A. Kaskas, M. Kebbiri, R. Kempley, A. Khaplanov, S. Klupp, M. Kogimtzis, I. Kojouharov, A. Korichi, W. Korten, T. Kröll, R. Krcken, N. Kurz, B. Ky, M. Labiche, X. Lafay, L. Lavergne, I. Lazarus, S. Leboutelier, F. Lefebvre, E. Legay, L. Legeard, F. Lelli, S. Lenzi, S. Leoni, A. Lermitage, D. Lersch, J. Leske, S. Letts, S. Lhenoret, R. Lieder, D. Linget, J. Ljungvall, A. Lopez-Martens, A. Lotodé, S. Lunardi, A. Maj, J. van der Marel, Y. Mariette, N. Marginean, R. Marginean, G. Maron, A. Mather, W. Męczyński, V. Mendéz, P. Medina, B. Melon, R. Menegazzo, D. Mengoni, E. Merchan, L. Mihailescu, C. Michelagnoli, J. Mierzejewski, L. Milechina, B. Million, K. Mitev, P. Molini, D. Montanari, S. Moon, F. Morbiducci, R. Moro, P. Morrall, O. Möller, A. Nannini, D. Napoli, L. Nelson, M. Nespolo, V. Ngo, M. Nicoletto, R. Nicolini, Y. L. Noa, P. Nolan, M. Norman, J. Nyberg, A. Obertelli, A. Olariu, R. Orlandi, D. Oxley, C. Özben, M. Ozille, C. Oziol, E. Pachoud, M. Palacz, J. Palin, J. Pancin, C. Parisel, P. Pariset, G. Pascovici, R. Peghin, L. Pellegri, A. Perego, S. Perrier, M. Petcu, P. Petkov, C. Petrache, E. Pierre, N. Pietralla, S. Pietri, M. Pignanelli, I. Piqueras, Z. Podolyak, P. L. Pouhalec, J. Pouthas, D. Pugnére, V. Pucknell, A. Pullia, B. Quintana, R. Raine, G. Rainovski, L. Ramina, G. Rampazzo, G. L. Rana, M. Rebeschini, F. Recchia, N. Redon, M. Reese, P. Reiter, P. Regan, S. Riboldi, M. Richer, M. Rigato, S. Rigby, G. Ripamonti, A. Robinson, J. Robin, J. Roccaz, J.-A. Ropert, B. Rossé, C. R. Alvarez, D. Rosso, B. Rubio, D. Rudolph, F. Saillant, E. Sahin, F. Salomon, M.-D. Salsac, J. Salt, G. Salvato, J. Sampson, E. Sanchis, C. Santos, H. Schaffner, M. Schlarb, D. Scraggs, D. Seddon, M. Åenyiit, M.-H. Sigward, G. Simpson, J. Simpson, M. Slee, J. Smith, P. Sona, B. Sowicki, P. Spolaore, C. Stahl, T. Stanios, E. Stefanova, O. Stézowski, J. Strachan, G. Suliman, P.-A. Söderström, J. Tain, S. Tanguy, S. Tashenov, C. Theisen, J. Thornhill, F. Tomasi, N. Toniolo, R. Touzery, B. Travers, A. Triossi, M. Tripon, K. Tun-Lanoë, M. Turcato, C. Unsworth, C. Ur, J. Valiente-Dobón, V. Vandone, E. Vardaci, R. Venturelli, F. Veronese, C. Veyssiere, E. Viscione, R. Wadsworth, P. Walker, N. Warr, C. Weber, D. Weisshaar, D. Wells, O. Wieland, A. Wiens, G. Wittwer, H. Wollersheim, F. Zocca, N. Zamfir, M. Zięblíński, A. Zucchiatti, Agata - advanced gamma tracking array, Nucl. Instrum. Methods A 668 (2012) 26. doi:https://doi.org/10.1016/j.nima.2011.11.081.

[27] A. Pullia, S. Capra, A low noise preamplifier for hpge detectors with auxiliary output for over range signal spectroscopy, 2015 IEEE Nuclear Science Symposium and Medical Imaging Conference (NSS/MIC) (2015) 1–2.

[28] A. Pullia, G. Pascovici, C. A. Ur, A versatile low-noise wide-range charge-sensitive preamplifier for hpge detectors, IEEE Nuclear Science Symposium Conference Record (2012) 815–818doi:10.1109/NSSMIC.2012.6551217.

[29] A. Pullia, D. Barrientos, D. Bazzacco, M. Bellato, D. Bortolato, R. Isocrate, A 12-channel 14/16-bit 100/125-ms/s digitizer with 24-gb/s optical output for agata/galileo, Proc. 2012 IEEE Nucl. Sci. Symp. Med. Imag. Conf. Rec. (2012) 819–823.

[30] D. Barrientos, Development of the control card for the digitizers of the second generation electronics of agata, Proc. 18th IEEE Real Time (RT) Conf. Rec. (2012) 1–3.

[31] D. Barrientos, Contributions to the new electronics of the agata gamma tracking detector. design, implementation, test and integration of the digitizers control card, Ph.D. thesis, Univ. Valencia, Spain (2013).

[32] D. Barrientos, M. Bellato, D. Bazzacco, D. Bortolato, P. Cocconi, A. Gadea, V. González, M. Gulmini, R. Isocrate, D. Mengoni, A. Pullia, F. Recchia, D. Rosso, E. Sanchis, N. Toniolo, C. A. Ur, J. J. Valiente-Dobón, Performance of the fully digital FPGA-based front-end electronics for the GALILEO array, IEEE Transactions on Nuclear Science 62 (6) (2015) 3134–3139. doi:10.1109/TNS.2015.2480243.

[33] Serial interface for data converters, JESD204A, JEDEC Solid State technology association (2006).

[34] M. Bellato, Global trigger and readout system for the agata experiment, IEEE Trans. Nucl. Sci. 55 (2008) 91–98.

[35] M. Bellato, D. Bortolato, J. Chavas, R. Isocrate, G. Rampazzo, A. Triossi, D. Bazzacco, D. Mengoni, F. Recchia, Sub-nanosecond clock synchronization and trigger management in the nuclear physics experiment AGATA, Journal of Instrumentation 8 (07) (2013) 07003. doi:10.1088/1748-0221/8/07/p07003.

[36] V. T. Jordanov, G. F. Knoll, A. C. Huber, J. A. Pantazis, Digital techniques for real-time pulse shaping in radiation measurements, Nucl. Instrum. Methods A 353 (1994) 261. doi:10.1016/0168-9002(94)91652-7.

[37] F. Recchia, D. bazzacco, M. Bellato, D. Bortolato, E. Farnea, D. Mengoni, Efficiency and energy resolution of the agata demonstrator at high count rate (2011).

[38] J. Gutleber, S. Murray, L. Orsini, Towards a homogeneous architecture for high-energy physics data acquisition sys-

tems, Computer Physics Communications 153 (2) (2003) 155. doi:https://doi.org/10.1016/S0010-4655(03)00161-9.

[39] S. Agostinelli, J. Allison, K. Amako, J. Apostolakis, H. Araujo, P. Arce, M. Asai, D. Axen, S. Banerjee, G. Barrand, F. Behner, L. Bellagamba, J. Boudreau, L. Broglia, A. Brunengo, H. Burkhardt, S. Chauvie, J. Chuma, R. Chytracek, G. Cooperman, G. Cosmo, P. Degtyarenko, A. Dell'Acqua, G. Depaola, D. Dietrich, R. Enami, A. Feliciello, C. Ferguson, H. Fesefeldt, G. Folger, F. Foppiano, A. Forti, S. Garelli, S. Giani, R. Giannitrapani, D. Gibin, J.J. Gómez Cadenas, I. González, G. Gracia Abril, G. Greeniaus, W. Greiner, V. Grichine, A. Grossheim, S. Guatelli, P. Gumplinger, R. Hamatsu, K. Hashimoto, H. Hasui, A. Heikkinen, A. Howard, V. Ivanchenko, A. Johnson, F. Jones, J. Kallenbach, N. Kanaya, M. Kawabata, Y. Kawabata, M. Kawaguti, S. Kelner, P. Kent, A. Kimura, T. Kodama, R. Kokoulin, M. Kossov, H. Kurashige, E. Lamanna, T. Lampén, V. Lara, V. Lefebure, F. Lei, M. Liendl, W. Lockman, F. Longo, S. Magni, M. Maire, E. Medernach, K. Minamimoto, P. Mora de Freitas, Y. Morita, K. Murakami, M. Nagamatu, R. Nartallo, P. Nieminen, T. Nishimura, K. Ohtsubo, M. Okamura, S. O'Neale, Y. Oohata, K. Paech, J. Perl, A. Pfeiffer, M. Pia, F. Ranjard, A. Rybin, S. Sadilov, E. D. Salvo, G. Santin, T. Sasaki, N. Savvas, Y. Sawada, S. Scherer, S. Sei, V. Sirotenko, D. Smith, N. Starkov, H. Stoecker, J. Sulkimo, M. Takahata, S. Tanaka, E. Tcherniaev, E. Safai Tehrani, M. Tropeano, P. Truscott, H. Uno, L. Urban, P. Urban, M. Verderi, A. Walkden, W. Wander, H. Weber, J. Wellisch, T. Wenaus, D. Williams, D. Wright, T. Yamada, H. Yoshida, D. Zschiesche, Geant4 – a simulation toolkit, Nucl. Instrum. Methods A 506 (2003) 250. doi:https://doi.org/10.1016/S0168-9002(03)01368-8.

[40] E. Farnea, F. Recchia, D. Bazzacco, T. Krll, Z. Podolyk, B. Quintana, A. Gadea, Conceptual design and monte carlo simulations of the agata array, Nuclear Instruments and Methods in Physics Research Section A: Accelerators, Spectrometers, Detectors and Associated Equipment 621 (1) (2010) 331 – 343. doi:https://doi.org/10.1016/j.nima.2010.04.043.

[41] C. Boiano, R. Bassini, A. Pullia, G. Benzoni, A. Bracco, S. Brambilla, F. Camera, F. Crespi, B. Million, O. Wieland, An advanced pulse stretcher for the acquisition of the "fast" component of baf_2 detectors signals, IEEE Transactions on Nuclear Science 53 (2) (2006) 444. doi:10.1109/TNS.2006.870178.

[42] C. Ghosh, V. Nanal, R. Pillay, K. Anoop, N. Dokania, S. Pal, M. Pose, G. Mishra, P. Rout, S. Kumar, D. Pandit, D. Mondal, S. Pal, S. Banerjee, P. J. Napiorkowski, O. Dorvaux, S. Kihel, C. Mathieu, A. Maj, Characterization of PARIS LaBr3(Ce) - NaI(Tl) phoswich detectors up to e $\sim$ 22 mev, Journal of Instrumentation 11 (2016). doi:10.1088/1748-0221/11/05/p05023.

[43] A. Maj, F. Azaiez, D. Jenkins, C. Schmitt, O. Stezowski, J. Wieleczko, D. Balabanski, P. Bednarczyk, S. Brambilla, F. Camera, D. Chakrabarty, M. Chełstowska, M. Ciemała, S. Courtin, M. Csatlos, Z. Dombradi, O. Dorvaux, J. Dudek, M. Erduran, S. Ertürk, B. Fornal, S. Franchoo, G. Georgiev, J. Gulyás, S. Harissopoulos, P. Joshi, M. Kiciska-Habior, M. Kmiecik, A. Krasznahorkay, G. A. Kumar, S. Kumar, M. Labiche, I. Mazumdar, K. Mazurek, W. Meczyński, S. Myalski, V. Nanal, P. Napiorkowski, J. Peyre, J. Pouthas, O. Roberts, M. Rousseau, J. Scarpaci, A. Smith, I. Stefan, J. Strachan, D. Watts, M. Zięblińnski, The paris project, Acta Physica Polonica B 40 (2009) 565.

[44] J.-M. Régis, G. Pascovici, J. Jolie, M. Rudigier, The mirror symmetric centroid difference method for picosecond lifetime measurements via $\gamma\gamma$ coincidences using very fast LaBr3(Ce) scintillator detectors, Nucl. Instrum. Methods A 622 (1) (2010) 83 – 92. doi:https://doi.org/10.1016/j.nima.2010.07.047.

[45] O. J. Roberts, A. M. Bruce, P. H. Regan, Z. Podolyk, C. M. Townsley, J. F. Smith, K. F. Mulholland, A. Smith, A labr3: Ce fast-timing array for DESPEC at FAIR, Nucl. Instrum. Methods A 748 (2014) 91 – 95. doi:https://doi.org/10.1016/j.nima.2014.02.037.

[46] M. Magalini, Lifetime measurements with fast-timing scintillators, bachelor thesis, Univ. Padova, Italy (2019).

[47] S. Capra, D. Mengoni, J. A. Duenas, P. R. John, A. Gadea, R. J. Aliaga, J.-J. Dormard, M. Assie, A. Pullia, Performance of the new integrated front-end electronics of the trace array commissioned with an early silicon detector prototype, Nucl. Instrum. Methods A 935 (4) (2019) 178. doi:10.1016/j.nima.2015.07.067.

[48] D. Mengoni, J. Dueñas, M.Assié, C. Boiano, P. John, R. Aliaga, D. Beaumel, S. Capra, A. Gadea, V. Gonzáles, A. Gottardo, L. Grassi, V. Herrero-Bosch, T. Houdy, I. Martel, V. Parkar, R. Perez-Vidal, A. Pullia, E. Sanchis, A. Triossi, J. V. Dobón, Digital pulse-shape analysis with a trace early silicon prototype, Nucl. Instrum. Methods A 764 (4) (2014) 241. doi:10.1016/j.nima.2014.07.054.

[49] N. Cieplicka-Orynczak, D. Mengoni, M. Ciemała, S. Leoni, B. Fornal, J. Duenas, S. Brambilla, C. Boiano, P. John, D. Bazzacco, G. Benzoni, G. Bocchi, S. Capra, F. Crespi, A. Goasduff, L. W. Iskra, G. Jaworski, F. Recchia, M. Siciliano, D. Testov, , J. Valiente-Dobón, Towards the lowest-energy limit for light ions identification with silicon pixel-type detectors, Eur. Phys. J. A 54 (4) (2018) 209. doi:10.1140/epja/i2018-12644-9.

[50] M. Rocchini, M. Chiari, E. Pasquali, A. Nannini, K. Hadyńska-Klęk, P. Sona, D. Bazzacco, G. Benzoni, F. Camera, C. Czelusniak, D. Doherty, A. Goasduff, P. John, M. Komorowska, N. Marchini, M. Matejska-Minda, B. Melon, D. Mengoni, P. Napiorkowski, M. Ottanelli, A. Perego, F. Recchia, M. Siciliano, L. Sottili, D. Testov, J. Valiente-Dobón, K. Wrzosek-Lipska, M. Zielińska, Applications of rutherford backscattering analysis methods to nuclear physics experiments, Nuclear Instruments and Methods in Physics Research Section B: Beam Interactions with

Materials and Atoms 486 (2021) 68. doi:https://doi.org/10.1016/j.nimb.2020.09.021.
[51] A. Nannini, M. Rocchini, K. Hadyńska-Klęk, N. Marchini, D. T. Doherty, M. Zielińska, M. Siciliano, A. Illana, M. Saxena, D. Bazzacco, G. Benzoni, F. Camera, M. Chiari, P. R. John, A. Goasduff, M. Komorowska, M. Matejska-Minda, D. Mengoni, P. Napiorkowski, D. R. Napoli, M. Ottanelli, A. Perego, F. Recchia, P. Sona, D. Testov, J. J. Valiente-Dobón, Coulomb excitation studies at LNL with the SPIDER-GALILEO set-up, Physica Scripta 95 (2) (2019) 024005. doi:10.1088/1402-4896/ab440f.
[52] W. Męczyński, P. Bednarczyk, J. Grębosz, J. Heese, M. Janicki, K. Maier, J. Merdinger, K. Spohr, M. Ziębliński, J. Styczeń, A detector for filtering -ray spectra from weak fusionevaporation reactions out of strong background and for doppler correction: The recoil filter detector, rfd, Nucl. Instrum. Methods A 580 (3) (2007) 1310. doi:https://doi.org/10.1016/j.nima.2007.07.132.
[53] C. Boiano, A. Guglielmetti, S. Riboldi, A 16 channels multi detector pulse shape amplifier with serialized readout, in: 2012 IEEE Nuclear Science Symposium and Medical Imaging Conference Record (NSS/MIC), 2012, pp. 865–867. doi:10.1109/NSSMIC.2012.6551228.
[54] J. J. Valiente-Dobón, G. Jaworski, A. Goasduff, F. J. Egea, V. Modamio, T. Hüyük, A. Triossi, M. Jastrzab, P.-A. Söderström, A. Di Nitto, G. De Angelis, G. De France, N. Erduran, A. Gadea, M. Moszyński, J. Nyberg, M. Palacz, R. Wadsworth, R. Aliaga, C. Aufranc, M. Bézard, G. Baulieu, E. Bissiato, A. Boujrad, I. Burrows, S. Carturan, P. Cocconi, G. Colucci, D. Conventi, M. Cordwell, S. Coudert, J. M. Deltoro, L. Ducroux, T. Dupasquier, S. Erturk, X. Fabian, V. González, A. Grant, K. Hadynska-Klek, A. Illana, M. L. Jurado-Gomez, M. Kogimtzis, I. Lazarus, L. Legeard, J. Ljungvall, G. Pasqualato, R. M. Pérez-Vidal, A. Raggio, D. Ralet, N. Redon, F. Saillant, B. Sayğı, E. Sanchis, M. Scarcioffolo, M. Siciliano, D. Testov, C. Stahl, M. Tripon, I. Zanon, Neda-neutron detector array, Nucl. Instrum. Methods A 927 (2019) 81–86. doi:https://doi.org/10.1016/j.nima.2019.02.021.
[55] P. Andreetto, F. Chiarello, F. Costa, A. Crescente, S. Fantinel, F. Fanzago, E. Konomi, P. Mazzon, M. Menguzzato, M. Segatta, G. Sella, M. Sgaravatto, S. Traldi, M. Verlato, L. Zangrando, Merging openstack-based private clouds: the case of cloudveneto.it, EPJ Web Conf. 214 (2019) 07010. doi:10.1051/epjconf/201921407010.

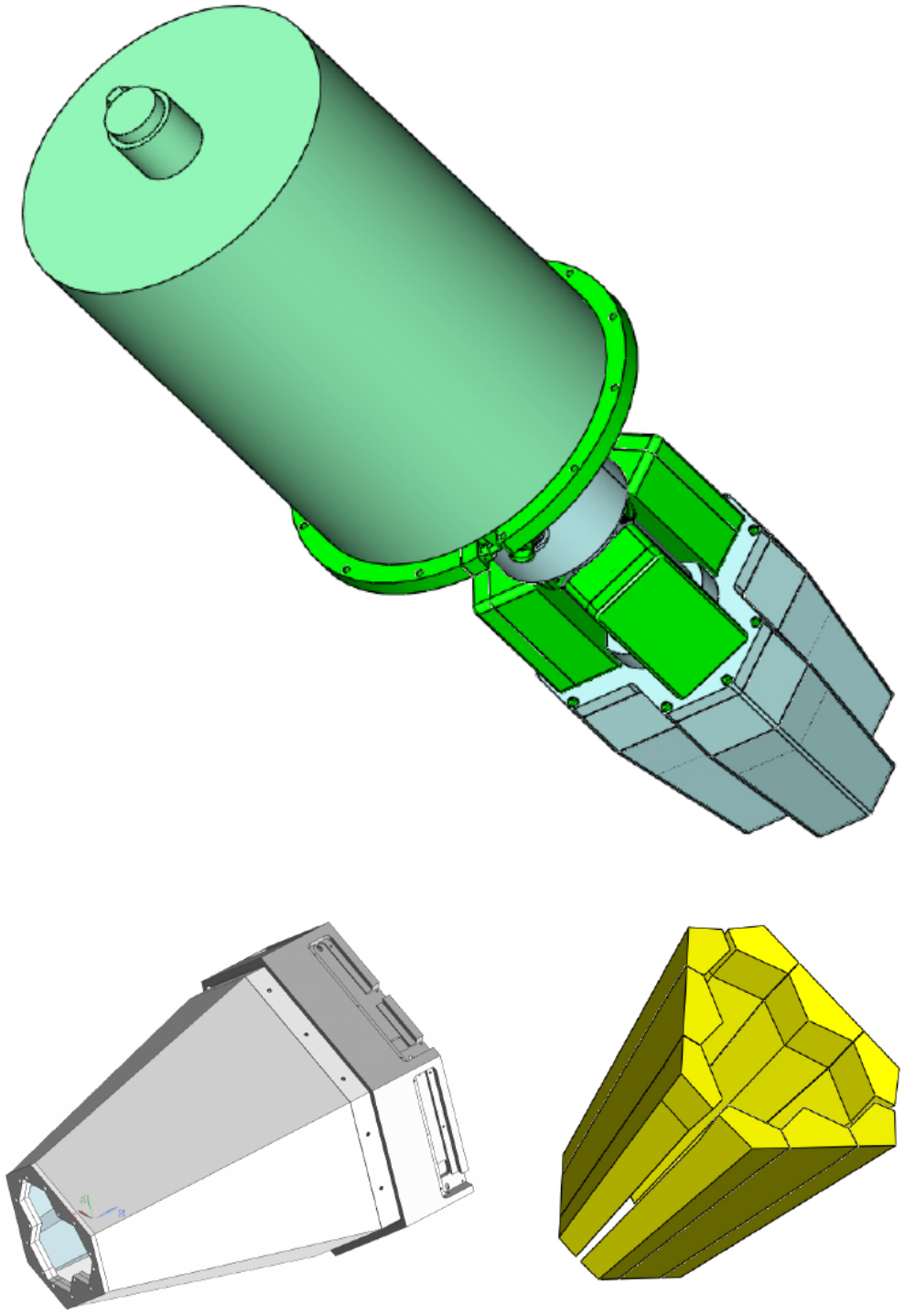

Figure 2: (Color Online) (Top panel) 3D rendering of GTC detector, seen from the back: the LN_2 dewar is depicted in light green while the HPGe capsules are shown in gray. (Bottom panel) Detailed view of the AC shields: the picture on the right shows, in yellow, the 3D rendering of the configuration of the BGO crystals, which are then enclosed in the endcap visible on the left.

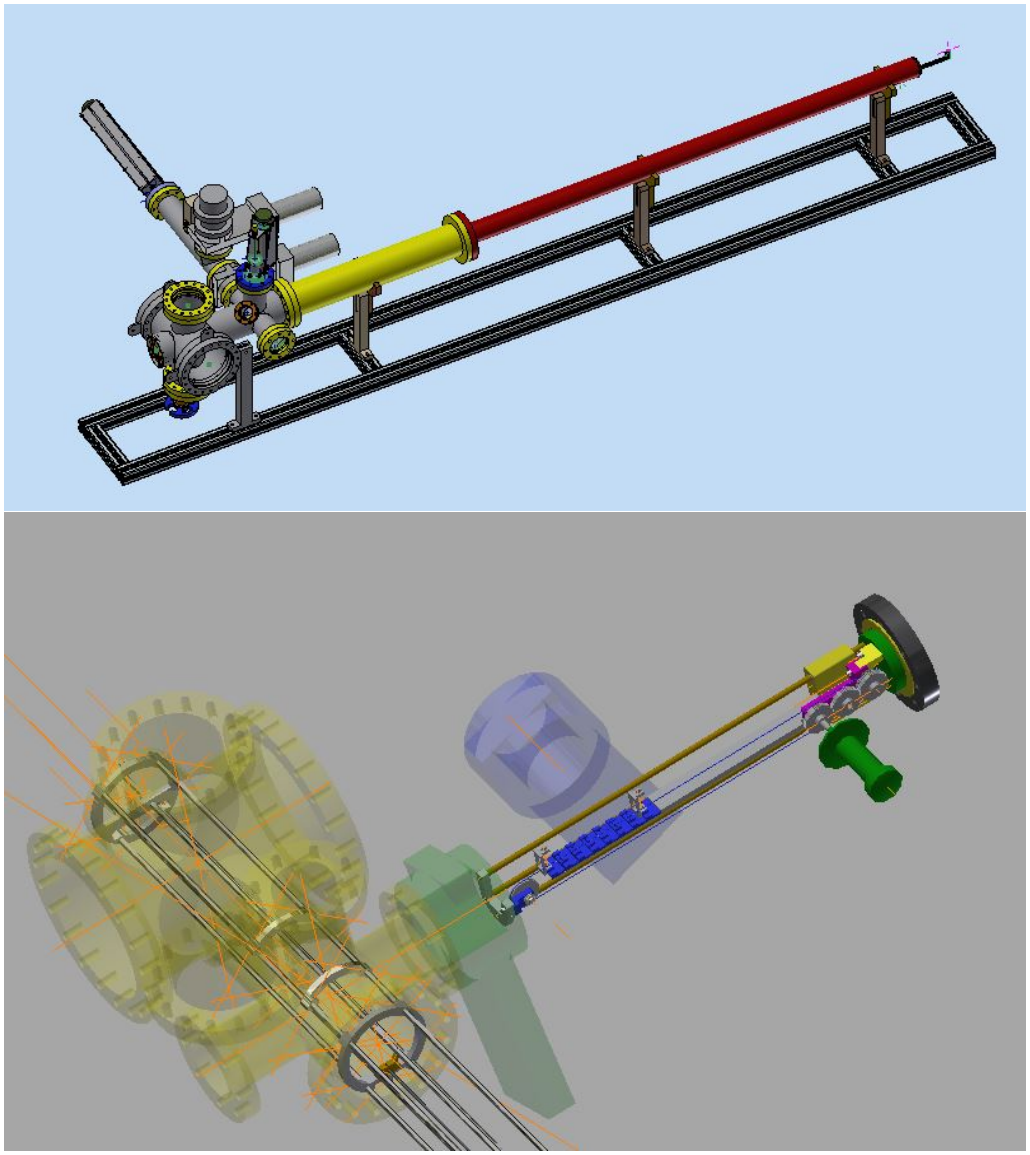

Figure 3: (Color Online) (Top Panel) 3D rendering of the downstream beamline including the remote handling system: one can note the manually controlled manipulator, represented in blue and extending above the beamline, and the chamber dedicated to the targets perpendicular to the beamline. At the far end one can see the stick extending towards the scattering chamber. (Bottom Panel) Detail of the interchange section and of the target chamber. In order to highlight construction elements the vacuum chambers are transparent.

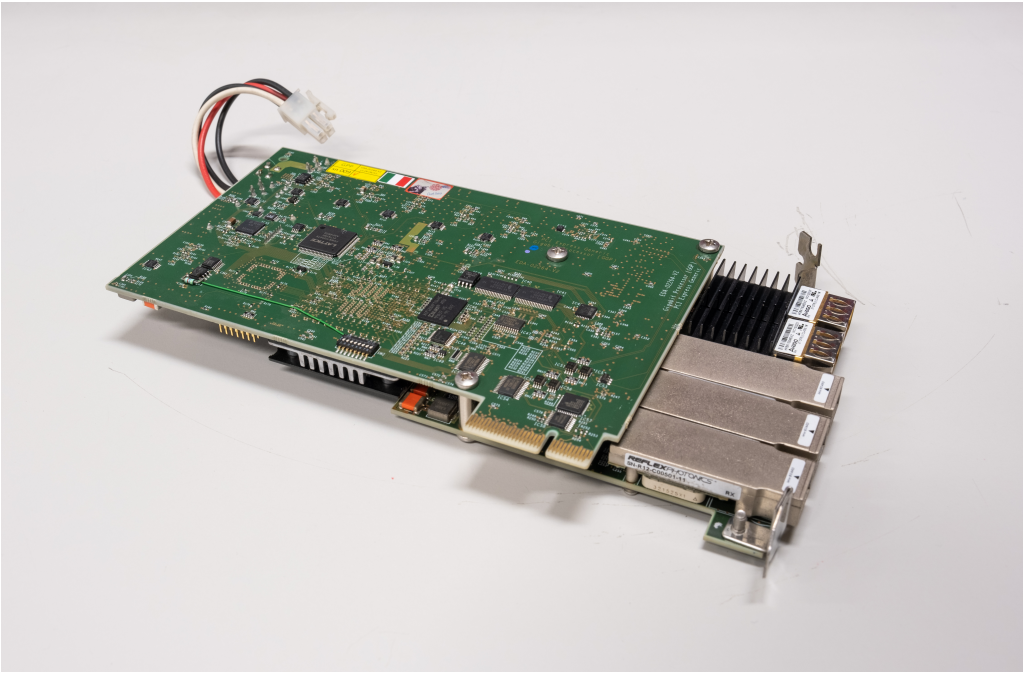

Figure 4: (Color Online) Picture of a Global Gigabit Processor (GGP) PCIe board. Digital signal are sent from the DigiOpt-12 boards to the GGP using the three MPO-12 optical fiber cables connected to the three lower SNAP-12 transceivers on the picture. The two additional ones (QSFP) are used for the clock distribution (top most) and the communication with the control board inside the digitzer (second transceiver).

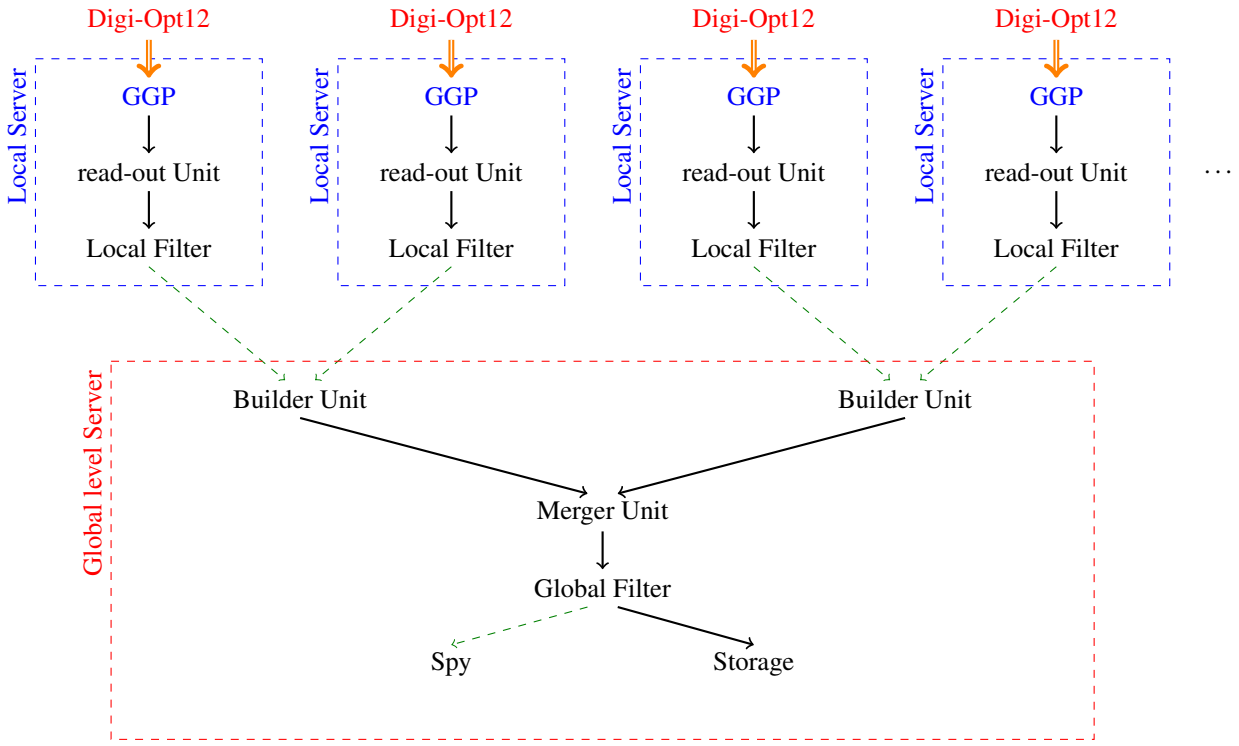

Figure 5: (Color Online) Block diagram representation of the DAQ, see text for details. Double (orange) arrows are for the optical links between the digitizer and the pre-processing board, full arrows are InfiniBand link while dashed (green) lines are for Ethernet links. The scheme represents the simplified version of the normal operation for GALILEO phase I. The DAQ can be scaled up to 12 Local servers to cover all the envisaged ancillaries. In this case up to 4 Builder Units can be inserted with up to 4 read-out units per Builder.

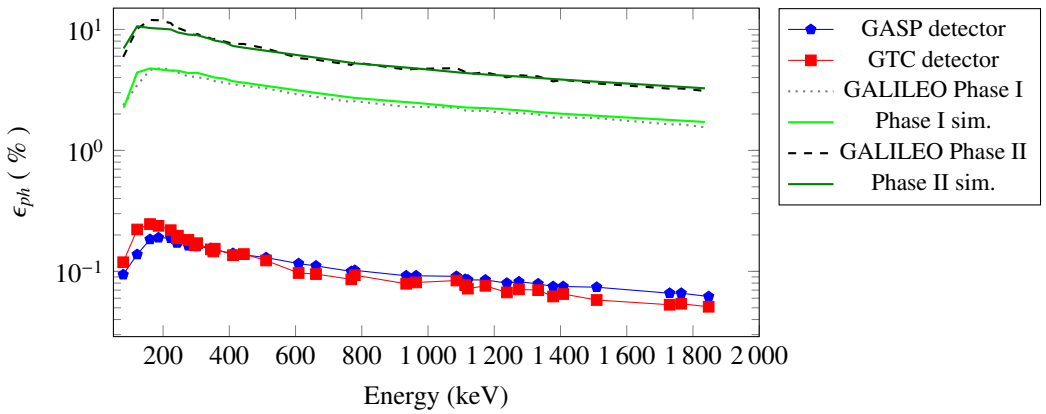

Figure 6: (Color Online) Comparison between the photo-peak efficiency of the tapered crystal (blue pentagons) and triple cluster crystal (red squares). Error bars are included in the points. For completeness the total efficiency of GALILEO in the phase I (dotted line) and Phase II (dashed line) are also reported. Simulated efficiencies of the two configurations are reported in green colors. See text for details.

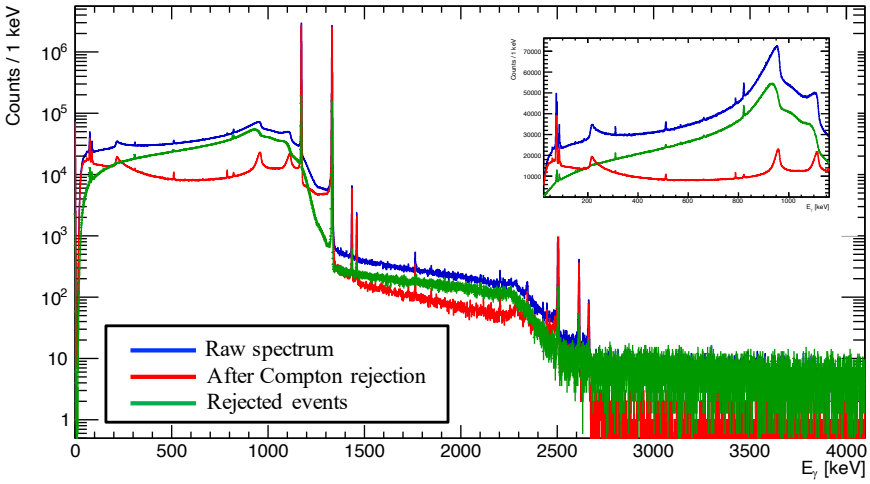

Figure 7: (Color Online) γ-ray spectra obtained with a ^{60}Co source placed at the center of the GALILEO array. The spectrum before Compton-scattering rejection (blue line) is compared to the one after Compton-scattering rejection (red). The events considered as Compton-scattered events (see text for details) are also represented (green). In the insert the energy region below the ^{60}Co source lines is depicted in linear scale to better assess the quality of the Compton background suppression.

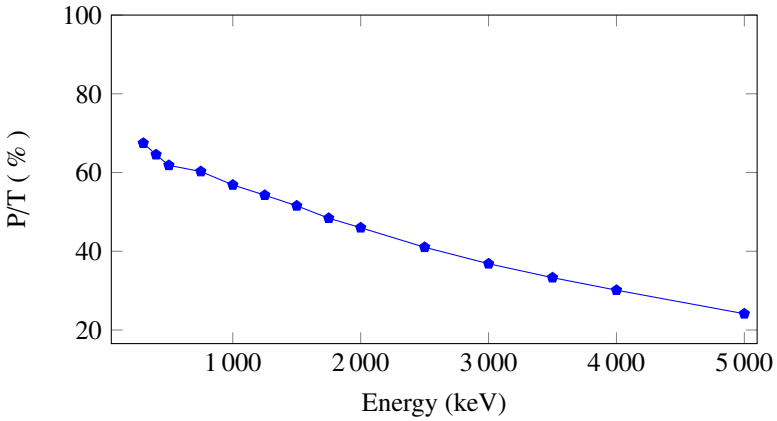

Figure 8: (Color Online) Evolution of the simulated P/T ratio as a function of the γ-ray energy for the tapered crystals.

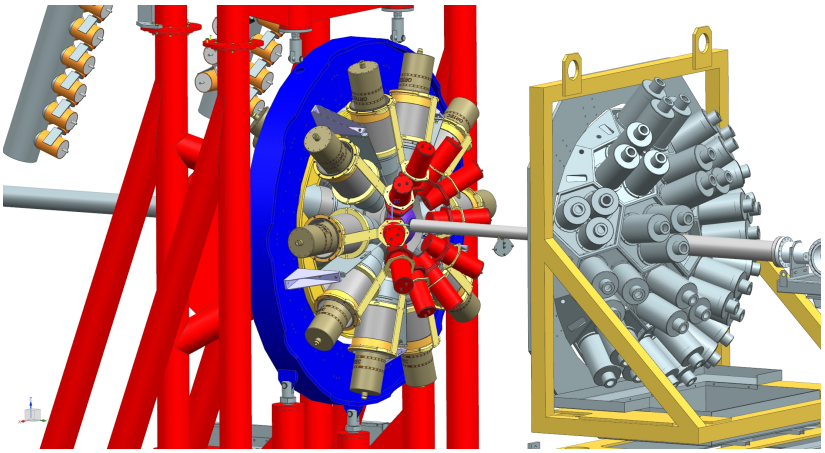

Figure 9: (Color Online) 3D rendering of the GALILEO array, Phase I configuration, coupled to $LaBr_3$:Ce detectors placed at 70°. The $LaBr_3$:Ce detector rendering, in red, includes also the housing of the photo-multiplier tubes. To the right of the figure the arrangement of the Neutron Wall with its mechanical structure is also visible.

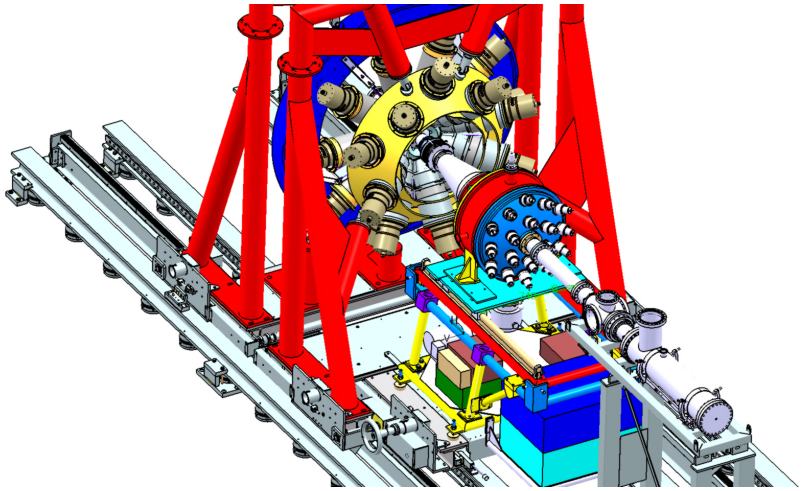

Figure 10: (Color Online) 3D rendering of the GALILEO array, Phase I configuration without backward ring, coupled with the Recoil Filter Detector (RFD). In the lower-right corner, the extended beam dump is also visible.

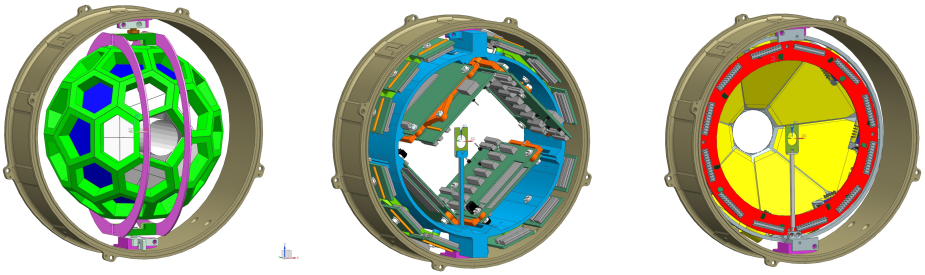

Figure 11: (Color Online) Light-charged particle and heavy ions silicon detectors, EUCLIDES, GALTRACE and SPIDER (from left to right), available to be combined with GALILEO for fusion-evaporation, direct and Coulomb excitation reactions.